Chapter 6B. Analysis of Imaging Spectrometer Data for the Dusar-Shaida Area of Interest

By Trude V.V. King

Abstract

Computer analysis of the HyMap spectroscopic data of the Dusar-Shaida area of interest (AOI) in the west-central part of Afghanistan used spectrum-matching techniques to identify the occurrence of selected surficial materials based on characteristic absorption features (absorption bands) in the HyMap data compared to a library of spectral standards. The HyMap data suggest that the AOI potentially has numerous previously unknown areas of mineralization, and the data suggests potential epithermal alteration and widespread oxidation within the AOI.

6B.1 Introduction

Previous U.S. Geological Survey (USGS) analyses of existing geologic data of Afghanistan revealed numerous areas with indications of potential mineral resources of various types (Peters and others, 2007). From these areas, several were selected for studies using hyperspectral remote sensing (imaging spectroscopy) data to characterize surface materials. One of those areas is the Dusar-Shaida area of interest (AOI) in western Afghanistan. The Dusar-Shaida AOI is approximately 674 km west of Kabul (fig. 6B–1) and is believed to have porphyry copper, volcanogenic massive sulfides, and tin-copper skarn deposits (Peters and others, 2007). To help assess these potential resources, high-resolution hyperspectral data were analyzed to detect the presence of selected minerals that may be indicative of past mineralization processes. This report contains the results of those analyses and identifies numerous sites within the Dusar-Shaida AOI that could merit further investigation, especially detailed geological mapping and geochemical studies.

6B.2 Data Collection and Processing

In 2007, imaging spectrometer (hyperspectral) data were acquired over most of Afghanistan as part of the U.S. Geological Survey (USGS) project "Oil and Gas Resources Assessment of the Katawaz and Helmand Basins." These data were collected to characterize surface materials in support of assessments of resources (coal, water, minerals, and oil and gas) and earthquake hazards in the country (King, Johnson, and others, 2010). Imaging spectrometers measure the reflectance of visible and near-infrared light from the Earth's surface in many narrow channels, producing a reflectance spectrum for each image pixel. These reflectance spectra can be interpreted to identify absorption features that result from specific chemical transitions and molecular bonds that provide compositional information about surface materials. Imaging spectrometer data can only be used to characterize the upper surface materials and not subsurface composition or structure. However, the results of subsurface processes can be indicated by the distribution of surface materials that can be detected using hyperspectral (imaging spectroscopy) data.

6B.2.1 Collection of Imaging Spectrometer Data

The HyMap imaging spectrometer (Cocks and others, 1998) was flown over Afghanistan from August 22 to October 2, 2007 (Kokaly and others, 2008). HyMap has 512 cross-track pixels and covers the wavelength range 0.43 to 2.48 micrometers (μm) in 128 channels. The imaging spectrometer was flown on a WB-57 high-altitude aircraft at approximately 50,000 ft. There were 207 standard data flight

lines and 11 cross-cutting calibration lines collected over Afghanistan for a total of 218 flight lines, covering a surface area of 438,012 km^2 (Kokaly and others, 2008). Data were received in scaled radiance format (calibrated to National Institute of Standards and Technology reference materials). Before processing, four channels that had low signal-to-noise ratios and (or) were in wavelength regions overlapped by adjacent detectors were removed from the image cubes. Each flight line was georeferenced to Landsat Thematic Mapper (TM) base imagery in UTM projection (Davis, 2007).

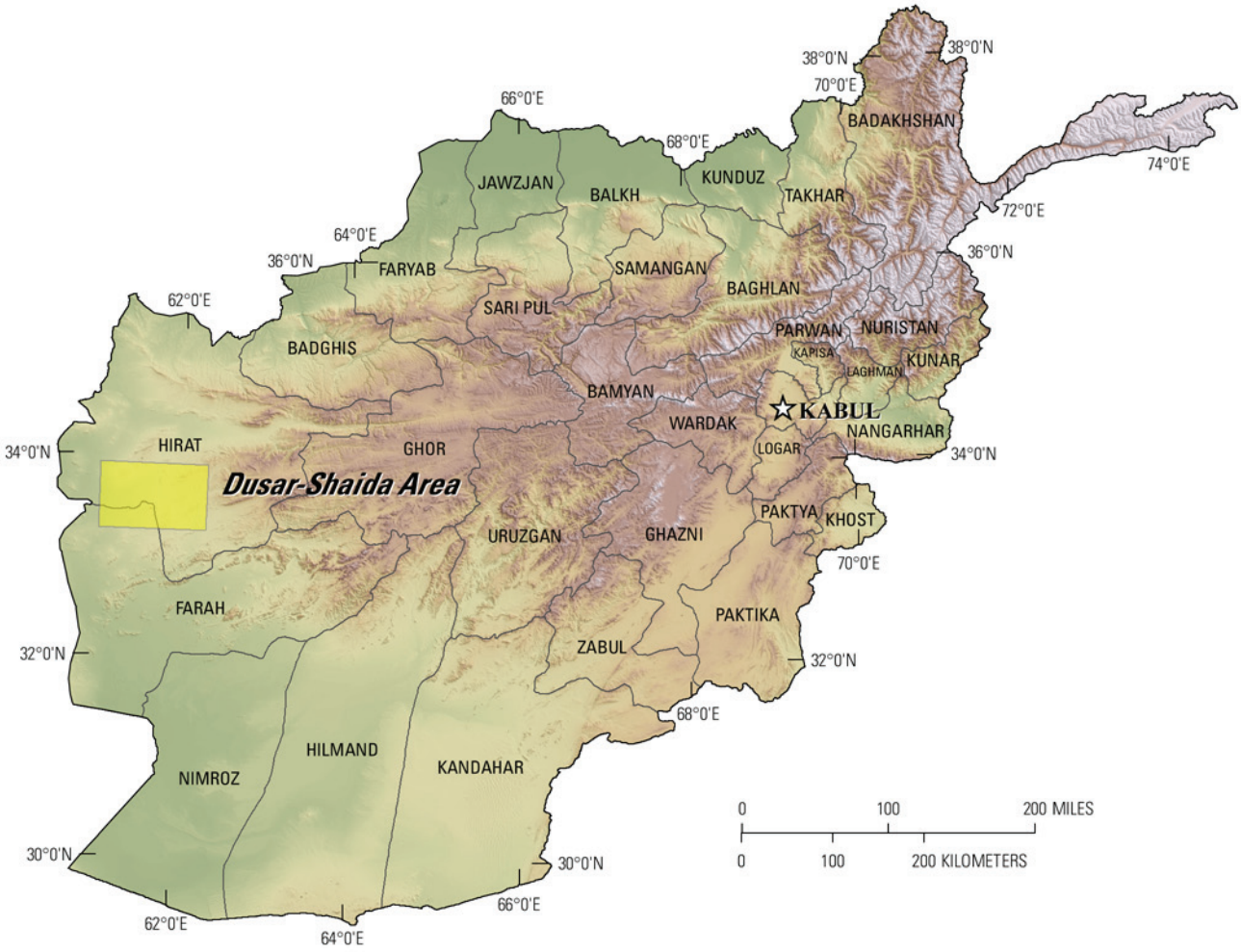

Figure 6B–1. The Dusar-Shaida area of interest is located approximately 674 km west of Kabul in the Farah and Hirat Provinces of Afghanistan.

6B.2.2 Calibration Process

HyMap data were converted from radiance to reflectance using a multi-step process. This calibration process removed the influence of the solar irradiance function, atmospheric absorptions, and residual instrument artifacts, resulting in reflectance spectra that have spectral features that arise from the material composition of the surface. Because of the extreme topographic relief and restricted access to ground-calibration sites, modifications to the typical USGS calibration procedures were required to calibrate the 2007 Afghanistan HyMap dataset (Hoefen and others, 2010). In the first step of the calibration process, the radiance data were converted to apparent surface reflectance using the radiative transfer correction program Atmospheric CORrection Now (ACORN; ImSpec LLC, Palmdale, Calif.). ACORN was run multiple times for each flight line, using average elevations in 100-m increments, covering the range of minimum to maximum elevation within the flight line. A single atmospherically corrected image was assembled from these elevation-incremented ACORN results. This was done by

determining the elevation of each HyMap pixel and selecting the atmospherically corrected pixel from the 100-m increment closest to that elevation.

Each assembled atmospherically corrected image was further empirically adjusted using ground-based reflectance measurements from a ground-calibration site. Spectra of five Afghanistan calibration sites were collected: field spectra from Kandahar Air Field, Bagram Air Base, and Mazar-e-Sharif Airport, as well as laboratory spectra of soil samples from two fallow fields in Kabul. These were used to calculate empirical correction factors using the pixels of atmospherically corrected HyMap data in the flight lines that passed over the sites. The empirical correction from the closest calibration site to each flight line was applied.

To further improve the data quality, an additional calibration step was taken to address the atmospheric differences caused, in part, by the large distances from calibration sites to where the HyMap data were acquired. The large distances were a result of the lack of safe access to ground-calibration sites. The duration of the airborne survey and variation in time of day during which flight lines were acquired also resulted in differences in atmospheric conditions between standard flight lines and lines over ground-calibration sites, which were used to derive the empirical correction factors. Over the course of the data collection, the sun angle, atmospheric water vapor, and atmospheric scattering differed for each flight line. To compensate for this, cross-cutting calibration flight lines over the ground-calibration areas were acquired (Kokaly and others, 2008) and used to refine data quality of standard data lines. A multiplier correction for each standard data line, typically oriented north-south, was derived using the pixels of overlap with the well-calibrated cross-cutting line that intersected it, subject to slope, vegetation cover, and other restrictions on pixel selection (Hoefen and others, 2010). As a result, the localized cross-calibration multiplier, derived from the overlap region, corrected residual atmospheric contamination in the imaging spectrometer data that may have been present after the ground-calibration step.

6B.2.3 Materials Maps and Presentation

After the calibration process, the reflectance data were georeferenced and then analyzed using Material Identification and Characterization Algorithm (MICA), a module of the USGS Processing Routines in Interactive Data Language (IDL) for Spectroscopic Measurements (PRISM) software (Kokaly, 2011). MICA compared the reflectance spectrum of each pixel of HyMap data against entries in a reference spectral library of minerals, vegetation, water, and other materials. The library included 97 reference spectra of well-characterized mineral and material standards. The resulting maps of material distribution, resampled to a 23×23 m^2 pixel grid, were used to prepare maps of mineral, vegetation, and other material occurrences.

MICA was applied to HyMap data twice to present the distribution of two categories of minerals that are naturally separated in the wavelength regions of their primary absorption features. MICA was applied using the subset of minerals with absorption features in the visible and near-infrared wavelength region, producing a 1-µm map of iron-bearing minerals and other materials (King, Kokaly, and others, 2011), and again using the subset of minerals with absorption features in the shortwave infrared, producing a 2-µm map of carbonates, phyllosilicates, sulfates, altered minerals, and other materials (Kokaly and others, 2011). For clarity of presentation, some individual classes in these two maps were bundled by combining selected mineral types (for example, all montmorillonites or all kaolinites) and representing them with the same color in order to reduce the number of colors required to represent the mineral classes.

The iron-bearing minerals map has 28 classes. Iron-bearing minerals with different mineral compositions but similar spectral features are difficult to classify as specific mineral species. Thus, generic spectral classes, including several minerals with similar absorption features, such as Fe^{3+} ,Type 1 and Fe^{3+} ,Type 2 are depicted on the map. The carbonate, phyllosilicates, sulfates, and altered minerals map has 32 classes. Minerals with slightly different mineral compositions but similar spectral features are less easily discriminated; thus, some identified classes consist of several minerals with similar

spectra, such as the chlorite or epidote class. When comparisons with reference spectra produced no viable match, a designation of "not classified" was assigned to a pixel.

6B.2.4 Data Limitations

It should be noted that geographic registration between various datasets is not always possible, because of differences in collection methods and resolution. The geographic accuracy and quality of each dataset is limited by the original source. Efforts were made to ensure the geographic accuracy of the HyMap data (Kokaly and others, 2008; Hoefen and others, 2010). However, exact registration between previously published known mineral occurrences, fault traces, geologic units, and structural boundaries in comparison to the HyMap data may not be ideal. To resolve additional details, the digital versions of these maps can be viewed at higher spatial resolution than what is possible in a single-page printed map.

6B.3 Geologic Setting of the Dusar-Shaida Area of Interest

The Dusar-Shaida AOI is located in the Hirat and Farah Provinces of Afghanistan (fig. 6B–1). The Dusar-Shaida AOI is approximately 8,619 km^2, and the two subareas, Dahana-Misgaran and Shaida, are approximately 171 km^2 and 334 km^2, respectively. The HyMap dataset only covers the eastern portion of the Dusar-Shaida AOI and does not include the Kaftar subarea. The elevation in the AOI ranges from 719 to 1,949 m and is cut by three rivers (fig. 6B–2). Numerous faults and fractures of different orientations (primarily striking northeast to southwest) are present in the area (fig. 6B–3). The rocks in the Landsat TM data range in color from very light gray, green, and red to very dark, bedded rock units. Colors in the TM image are generally related to specific geologic units (fig.6B–4), however, there are exceptions.

6B.3.1 Lithology and Structure

The Dusar-Shaida AOI has stratified rocks that range in age from Early Jurassic to Recent and intrusive rocks of Early Cretaceous, Eocene-Oligocene, and Oligocene age (fig. 6B–4; Doebrich and others, 2006; Abdullah and Chmyriov, 1977). The intrusive rocks are exposed in the western and northern part of the AOI.

6B.3.2 Known Mineralization

Figure 6B–5 shows 12 locations where reconnaissance field geology and the geologic literature have identified potential areas of mineralization. The locations of the mineral resources are also shown on some of the topical maps for the Dusar-Shaida AOI and two subareas (Dahana-Misgaran and Shaida) to illustrate how these mineralized sites are reflected in the HyMap data. The mineralogical characteristics of the sites are summarized in table 6B–1. The mineralization occurrences include (1) polymetallic veins, (2) skarn copper (Cu), (3) vein tin (Sn), (4) skarn Sn, and (5) volcanogenic massive sulfide deposits.

The geology of the Dusar-Shaida AOI has been reported (Peters and others, 2007; Doebrich and others, 2006) to include granite, granodiorite, quartz syenite, granosyenite, and volcanic rocks. Within the Dusar-Shaida AOI, the unclassified Kalmurgh mineral deposit (fig. 6B–5) is a base-metal occurrence hosted in Lower Cretaceous limestone, in a narrow zone containing disseminated chalcopyrite, pyrite, malachite, and azurite (Dronov and others, 1972; Peters and others, 2007).

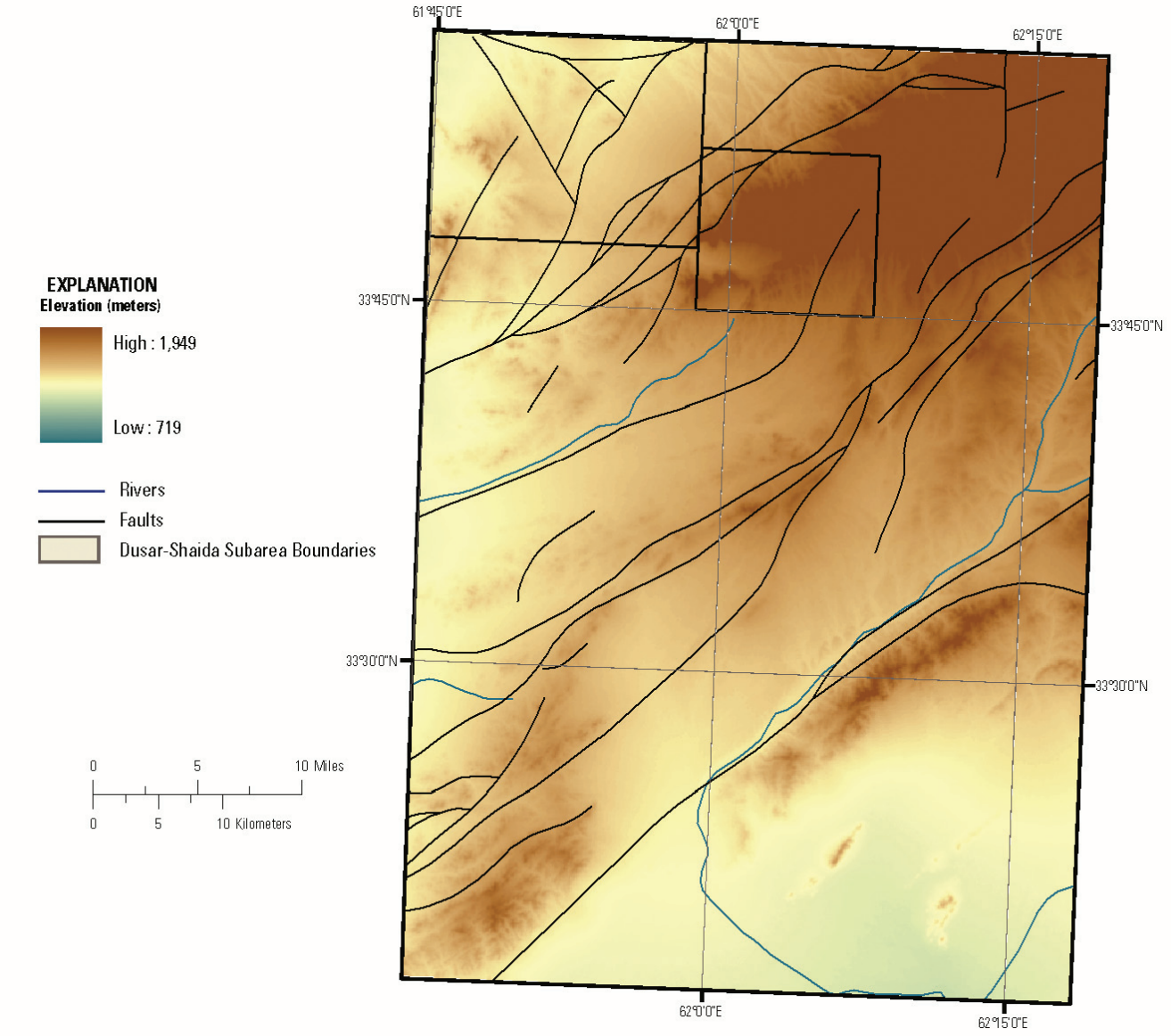

Figure 6B–2. Elevations and topography of the Dusar-Shaida area of interest (AOI). The AOI is cut by three rivers.

The Sardakhana copper skarn (lat 33°25′N., long 61°48′E.; fig. 6B–5) occurs in Lower Cretaceous deposits intruded by Eocene–Oligocene granites. According to Peters and others (2007), the skarns and surrounding rocks are intersected by diabase porphyry rocks of Miocene age. The skarns consist of garnet, iron hydroxides, and disseminated malachite and chalcopyrite.

In the Shaida subarea, the rocks are extensively altered and intruded by numerous dikes and sheets (Peters and others, 2007). The Shaida prospects are associated with a Upper Jurassic to Lower Cretaceous quartz porphyry and Jurassic quartz keratophyre volcanic rocks that have been intruded by Oligocene fine-grained granite and dikes and sheets of granite porphyry (Peters and others, 2007; fig. 6B–13).

The Dahana-Misgaran subarea is reported to contain tin-bearing skarn and vein mineral occurrences associated with Eocene–Oligocene age plutons. The subarea includes several mineral occurrences including Misgaran (tin skarn), Mir-Ali (copper), East Mistaron (tin skarn), Dacite (tin vein), Bandi-Medira (tin vein), and Dahana (copper skarn) (fig. 6B–24).

The Bandi-Medira occurrence is hosted in Oligocene granite and has associated tourmaline veins and zones containing cassiterite, magnetite, cheelite, galena, and chalcopyrite (Peters and others, 2007). In the southern part of the Bandi-Medira area along the contact of the pluton, copper-oxide materials and zones of disseminated chalcopyrite are present.

The Dacite occurrence consists of three mineralized zones in Oligocene granite and Eocene–Oligocene volcanic rocks with anomalous concentrations of lead, zinc, copper, and arsenic (Peters and others, 2007).

The Dahana copper skarn occurs in Lower Cretaceous rocks and contains zones of magnetite and sulfide minerals, tin, copper, and lead (Peters and other, 2007).

The Misgaran occurrence is in Lower Cretaceous rocks (siltstone, sandstone, shale, and limestone) in contact with Oligocene granite. A mineralized zone contains copper, magnetite, and tin. A variety of ore types such as veinlet-disseminated, massive, and limonite-hematite brecciated textures are present. Limonite-hematite and massive sulfide zones are also recognized (Peters and others, 2007).

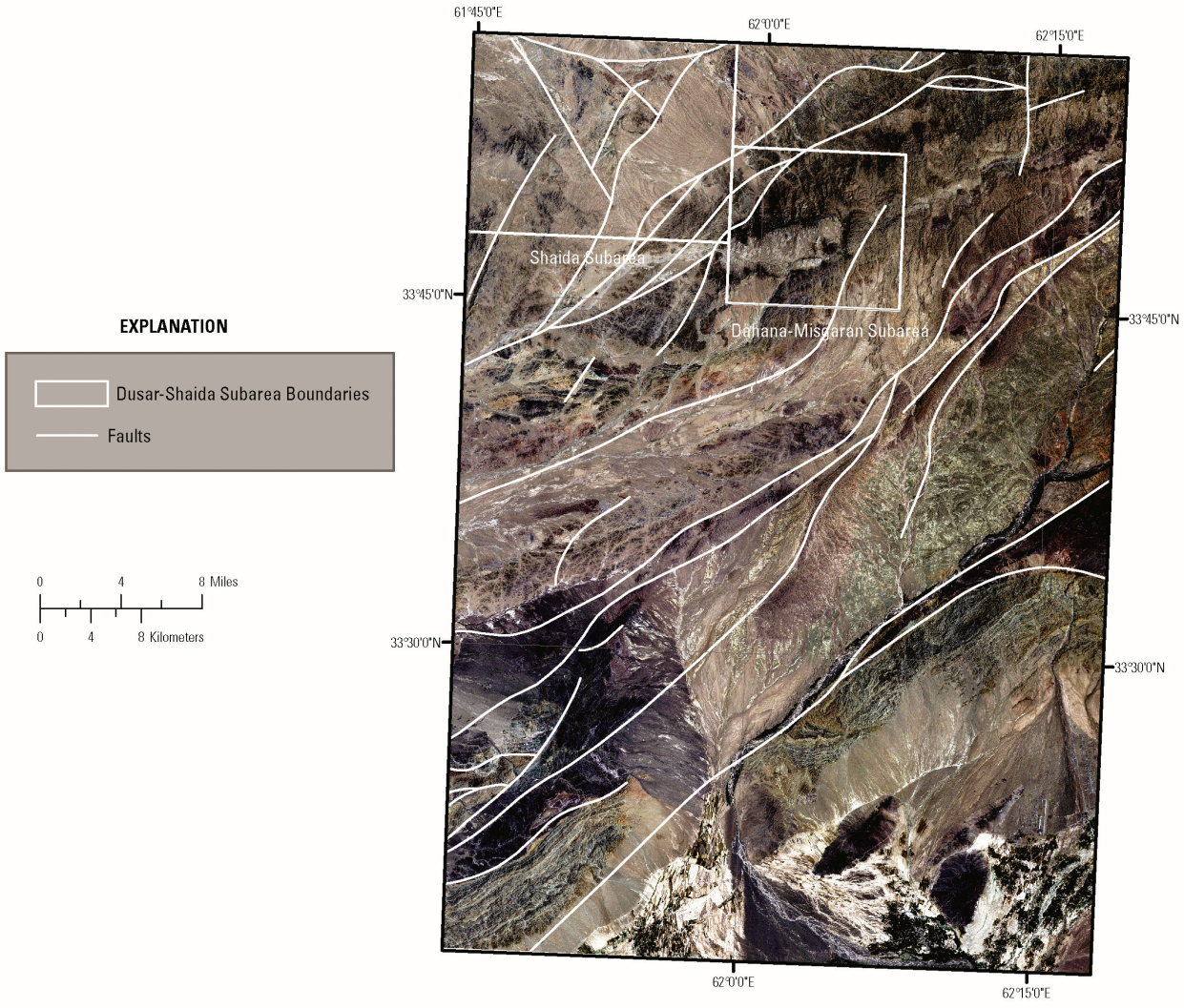

Figure 6B–3. Numerous faults and fractures of different orientation occur within the Dusar-Shaida area of interest (AOI). The fault traces (Peters and others, 2007) are shown on a Landsat Thematic Mapper image (Davis, 2007). The map shows the AOI and two subareas: Shaida and Dahana-Misgaran.

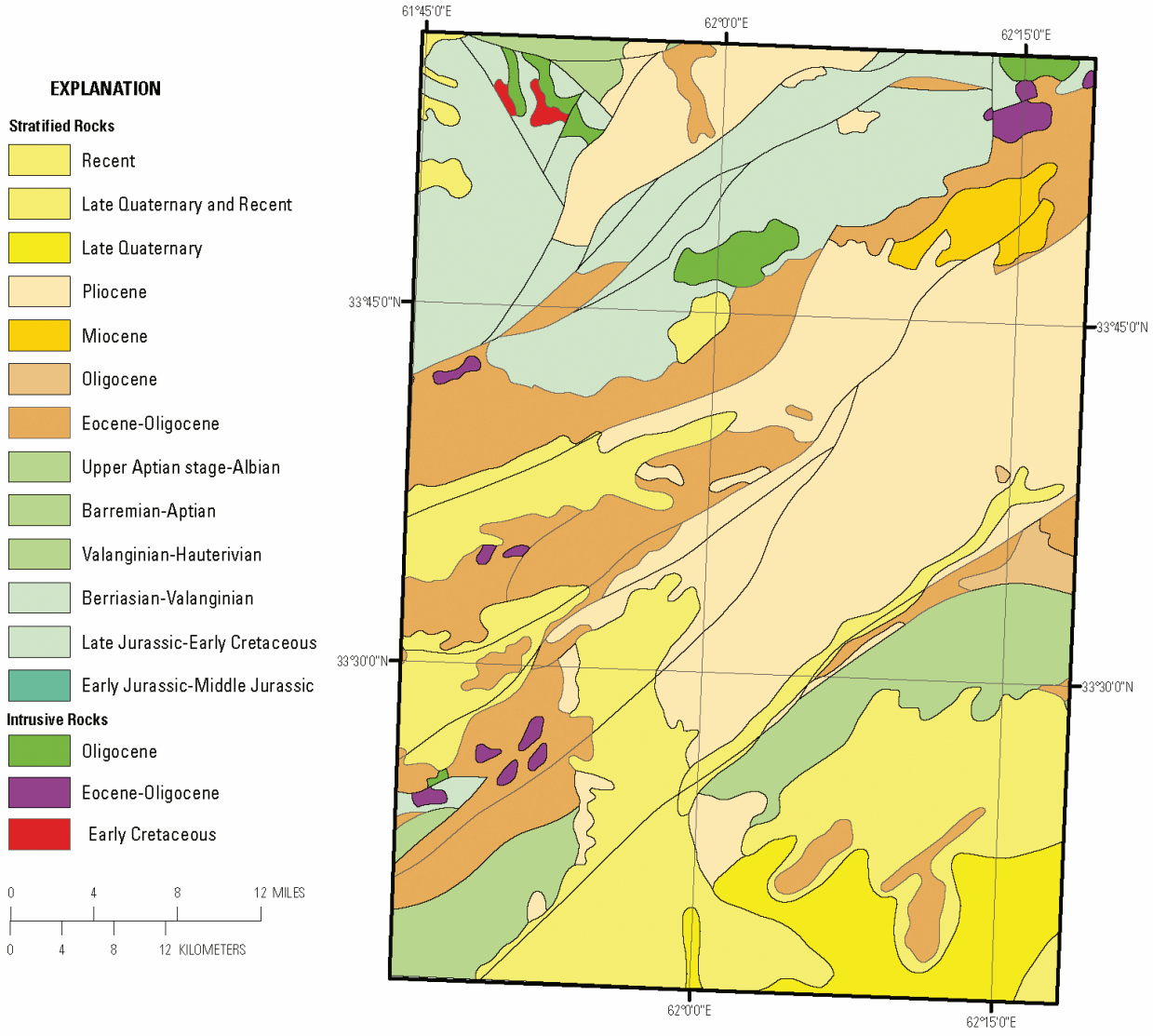

Figure 6B–4. Geologic map of the Dusar-Shaida area of interest taken from Doebrich and others (2006).

6B.4 Mineral Maps of the Dusar-Shaida Area of Interest

Analysis of the HyMap imaging spectrometer data of the Dusar-Shaida AOI using spectroscopic methods resulted in the identification of a wide variety of minerals exposed at the surface. Although the occurrence of certain minerals may suggest that mineralization processes may have once operated in the area, many of the minerals that were identified are also common rock-forming minerals or minerals that can be derived from the weathering of a wide variety of rock types. Consequently, the distribution patterns of the identified minerals and the geologic context in which they occur are extremely important in understanding the causes of mapped mineral occurrences and evaluating the possible potential for related mineral deposits.

Table 6B–1. Known sites of mineralization in the Dusar-Shaida area of interest.

[Data are from Peters and others (2007)]

Name	Deposit type	Mineralogy	Gangue	Alteration
Sardakhana	Skarn Cu	Malachite; chalcopyrite; iron hydroxide	Garnet; vesuvianite	Skarn alteration of garnet-vesuvianite facies
Kalmurgh	Unclassified	Chalcopyrite; pyrite; malachite; azurite	No data	_
Dahana	Skarn Cu	Magnetite; chalcopyrite	No data	Skarn alteration
Dacite	Vein Sn	Cassiterite	Quartz; tourmaline	Quartz-tourmaline alteration
Bandi-Medira (Daghana)	Vein Sn	Cassiterite; magnetite; scheelite; galena; pyrite; chalcopyrite	Quartz; tourmaline; garnet; diopside; vesuvianite; epidote; ankerite	Quartz-tourmaline alteration; tourmalinization; skarn alteration of garnet-diopside facies; skarn alteration of diopside-vesuvianite facies; skarn alteration
East (Mistaron)	Skarn Sn	Pyrrhotite; magnetite; galena; sphalerite; arsenopyrite; chalcopyrite; cassiterite; stannite; marcasite; pyrite; cassiterite; hematite; cerussite	Garnet; diopside; chlorite; quartz;	Skarn alteration of garnet-diopside facies; skarn alteration of calc types; chloritization; silicification; limonitization
Misgaran	Skarn Sn	–	–	–
Shaida II	Unknown Cu	Limonite; malachite	Quartz	Silicification; limonitization
Shaida III	Unknown Cu	Chalcopyrite; azurite	Quartz	Silicification; limonitization
Shaida	Volcanogenic massive sulfide	Limonite; hematite; secondary mineral of copper; pyrite; pyrrhotite; sphalerite; chalcopyrite	No data	Limonitization
Shaida I	Polymetallic vein	Limonite; malachite; azurite; chalcopyrite	Quartz	Silicification; limonitization
Mir-Ali	Polymetallic vein	Malachite; azurite; chalcopyrite; pyrite	Quartz; epidote; fluorite	Silicification; epidotization

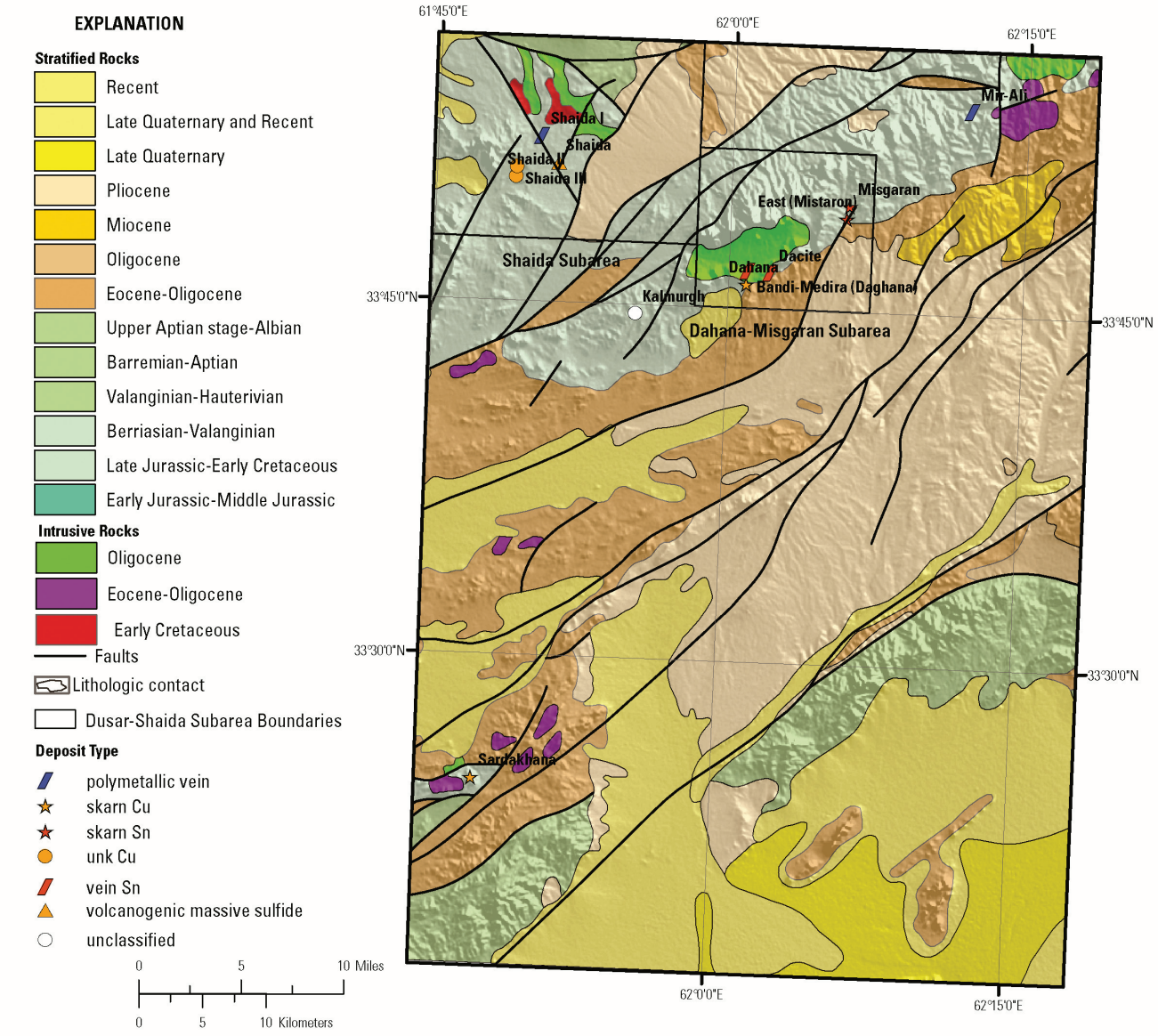

Figure 6B–5. Location of known mineral occurrences in the Dusar-Shaida area of interest. The map consists of four data layers: shaded relief base map, transparency of the geologic map (Doebrich and others, 2006), fault traces (Peters and others, 2007), and known mineral occurrences (Peters and others, 2007). Unk, unknown.

Figures 6B–6 and 6B–7 show the distribution of the iron-bearing minerals (28 possible classes) and carbonates, phyllosilicates, sulphates, altered minerals, and other materials (32 possible classes) for the Dusar-Shaida AOI. To enhance visualization of the subtleties of the mineral distribution patterns in these classified image maps, a series of topical images depicting groups of minerals that are commonly related or occur together in special geologic environments have been produced. Figure 6B–8 shows the distribution of carbonate minerals in the AOI, and figure 6B–9 shows where the clays and micas were mapped. The distribution of iron-oxide and iron-hydroxide minerals is displayed in figure 6B–10. Secondary minerals are shown in figure 6B–11 and minerals commonly found in hydrothermally altered rocks are mapped in figure 6B–12.

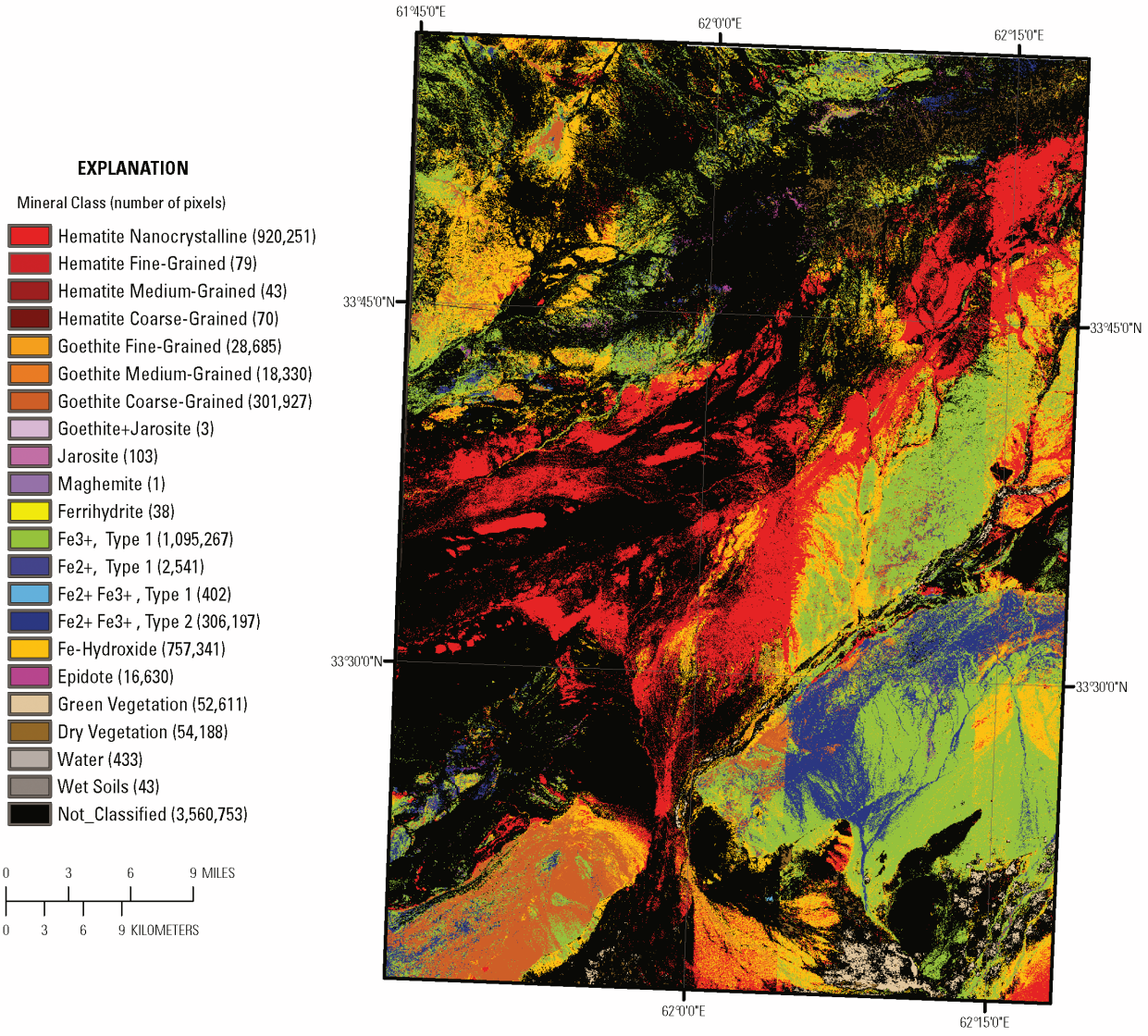

Figure 6B–6. Image showing iron-bearing and other minerals in the Dusar-Shaida area of interest detected by the HyMap data.

6B.4.1 Carbonate Minerals

The calcite and calcite + muscovite/illite mineral groups make-up more than 90 percent of the mapped material and are continuous across most geologic boundaries. The widespread occurrence of carbonate minerals limits their usefulness for detecting areas characterized by calcite alteration (fig. 6B–8). Although difficult to see because of the relatively small number of pixels, dolomite and dolomite mineral mixtures are present throughout the area, with small concentrations in the southeastern corner (lat 32°18′14.67″N., long 62°16′10.05″E.) of the AOI in late Quaternary and Recent units. Iron carbonates are associated with the Berriasian–Valanginian age rocks in the northern third of the image and in the late Quaternary units in the southeastern part of the AOI. The linear pattern of Fe-carbonates near (lat 33°23′14.24″N., long 62°15′24.34″E.) is known to be related to the infrastructure at the Shindand Airfield.

The Sardakhana copper skarn (lat 33°25′N., long 61°48′E.) and the Kalmurgh base-metal deposit occur in areas dominated by the presence of calcite.

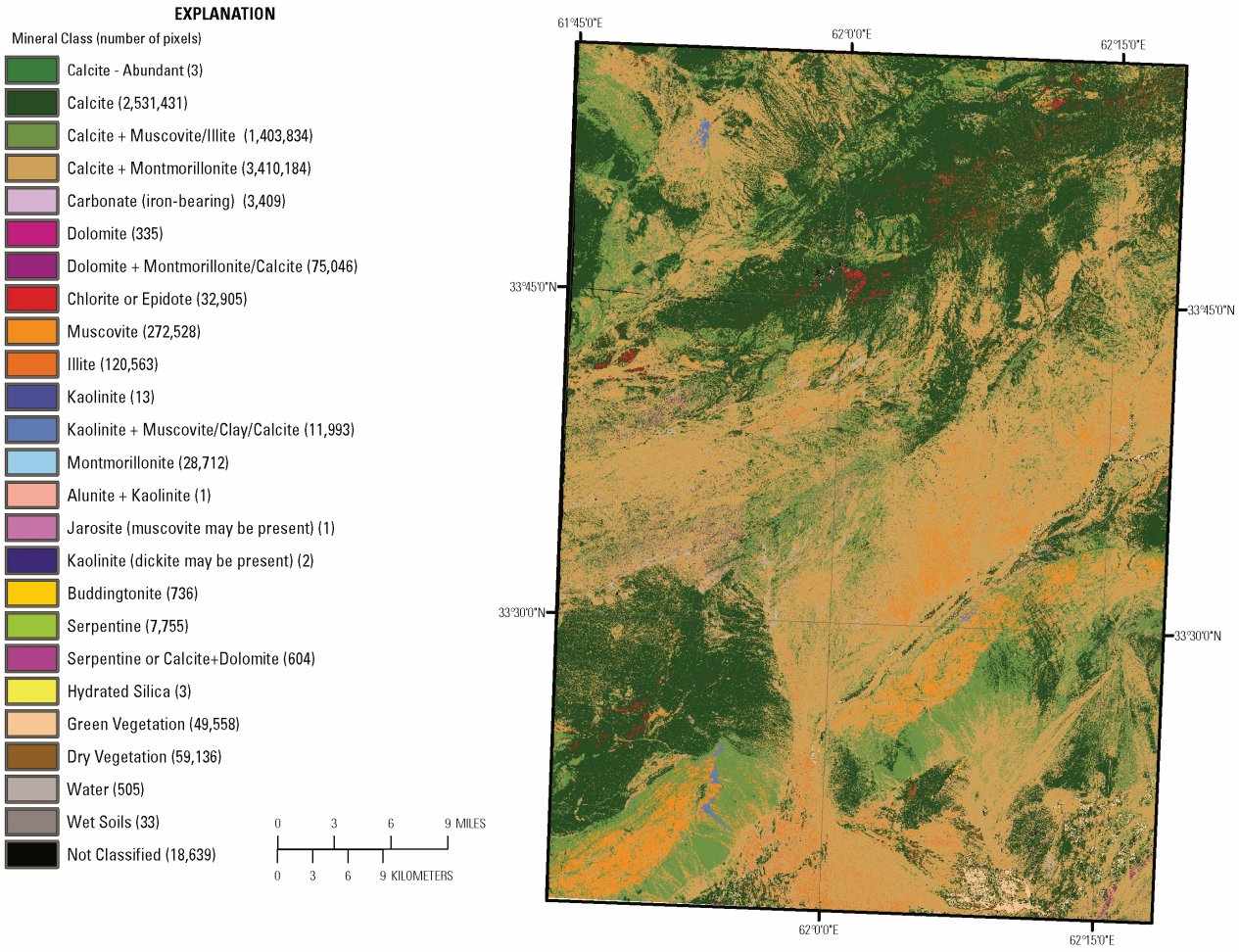

Figure 6B–7. Distribution of clays, carbonates, phyllosilicates, sulphates, and other alteration minerals detected in the HyMap data for the Dusar-Shaida area of interest.

6B.4.1.1 Clays and Micas

The phyllosilicates are the second-most abundant mineral group mapped in the AOI (fig. 6B–9). Muscovites and illites are the dominate minerals. Although the muscovite pixels are scattered over much of the AOI, the largest concentration occurs in Valanginian–Hauterivian and Pliocene age rocks in the southern part of the area. Illite pixels are widely scattered over the entire AOI, but show heavier concentrations in Quaternary and Recent rocks in the southern part of the area. The largest concentration of epidote and chlorite occurs in the northern half of the AOI in rocks of Barremian–Aptian and Eocene–Oligocene age. Small spatial concentrations of these minerals also occur near the Sardakhana copper skarn prospect in Eocene–Oligocene rocks.

The kaolinite pixels primarily map near the contact zone of the Valanginian–Hauterivian, Eocene–Oligocene, and Pliocene rocks in the southwestern part of the area. An additional cluster of kaolinite-rich material occurs in the northwestern part of the AOI in the Shaida subarea (fig. 6B–20). Although montmorillonite pixels are spatially scattered over the AOI, a small spatially distinct group occurs along fault traces in Eocene–Oligocene (lat 33°31′17.87″N., long 61°47′57.85″E.) and Quaternary–Recent (lat 33°41′23.36″N., long 61°59′46.18″E.) rocks. Montmorillonite pixels occur spatially along mapped fault traces in Pliocene age rocks (lat 33°52′36.34″N., long 62°12′49.54″E.), in a linear trend in Eocene–Oligocene age rocks (lat 33°52′36.34″N., long 62°12′49.54″E.) near the Eocene-Oligocene intrusion, and in late Quaternary and Recent rocks in the southeastern corner of the area

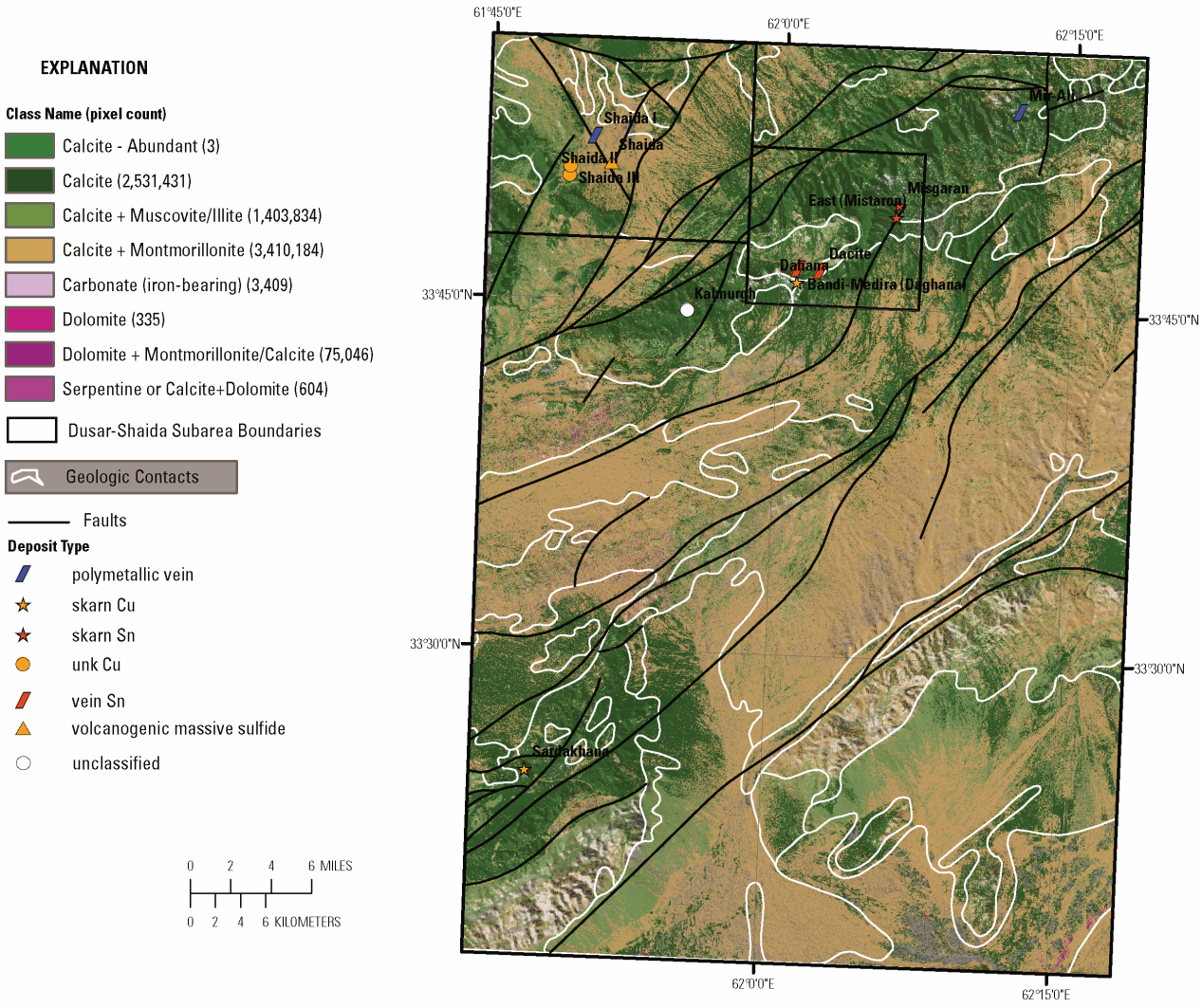

Figure 6B–8. Distribution of carbonate-bearing minerals detected in the Dusar-Shaida area of interest by the HyMap. Calcite and montmorillonite mixtures are the dominant mineral groups in the area. Unk, unknown.

6B.4.1.2 Iron Oxides and Iron Hydroxides

Figure 6B–10 shows the iron-bearing and other alteration minerals in the Dusar-Shaida AOI. Hematites, Fe-hydroxides, and goethitic pixels dominate the AOI. Hematitic minerals occur in a southwest to northeast trend in the center of the area in Pliocene, Eocene–Oligocene, and Miocene rocks. The widespread spatial distribution of hematite and Fe-hydroxide pixels is common in Pliocene rocks. Well-defined hematite (without associated Fe-hydroxides) occurs in spatially consistent patterns in Eocene–Oligocene and Quaternary–Recent rocks in the western half of the AOI. Iron-hydroxides with minor amounts of hematitic and goethitic mineral pixels show a spatial preference for the Berriasian–Valanginian rocks in the northern part of the AOI and in late Quaternary and Recent rocks near (lat 33°30′N., long 62°15′E.). A goethitic-rich cluster of minerals (associated with minor amounts of hematite and Fe-hydroxide) occurs in the southwestern corner of the area. Epidotes show spatially consistent patterns in the Barremian–Aptian and Eocene–Oligocene rocks in the northern part of the area. A ring of epidote appears in close proximity to the Oligocene intrusion near lat 33°47′2.0″N., long 62°0′55.74″E. in Berriasian–Valanginian rocks.

The area surrounding the Sardakhana prospect has scattered epidote, Fe-hydroxide, and goethitic minerals.

6B.4.1.3 Common Secondary Minerals

The occurrence and distribution of common secondary minerals for the AOI are shown in figure 6B–11. Epidote and chlorite minerals are mapped primarily in the Berriasian–Valanginian and Eocene-Oligocene rocks in northern half of the AOI. Chlorite or epidotes are also mapped near the Sardakhana prospect. The Kalmurgh occurrence has only pixels of epidote present. Scattered pixels of serpentine minerals occur over the entire area, but no significant spatial clustering of pixels is noted.

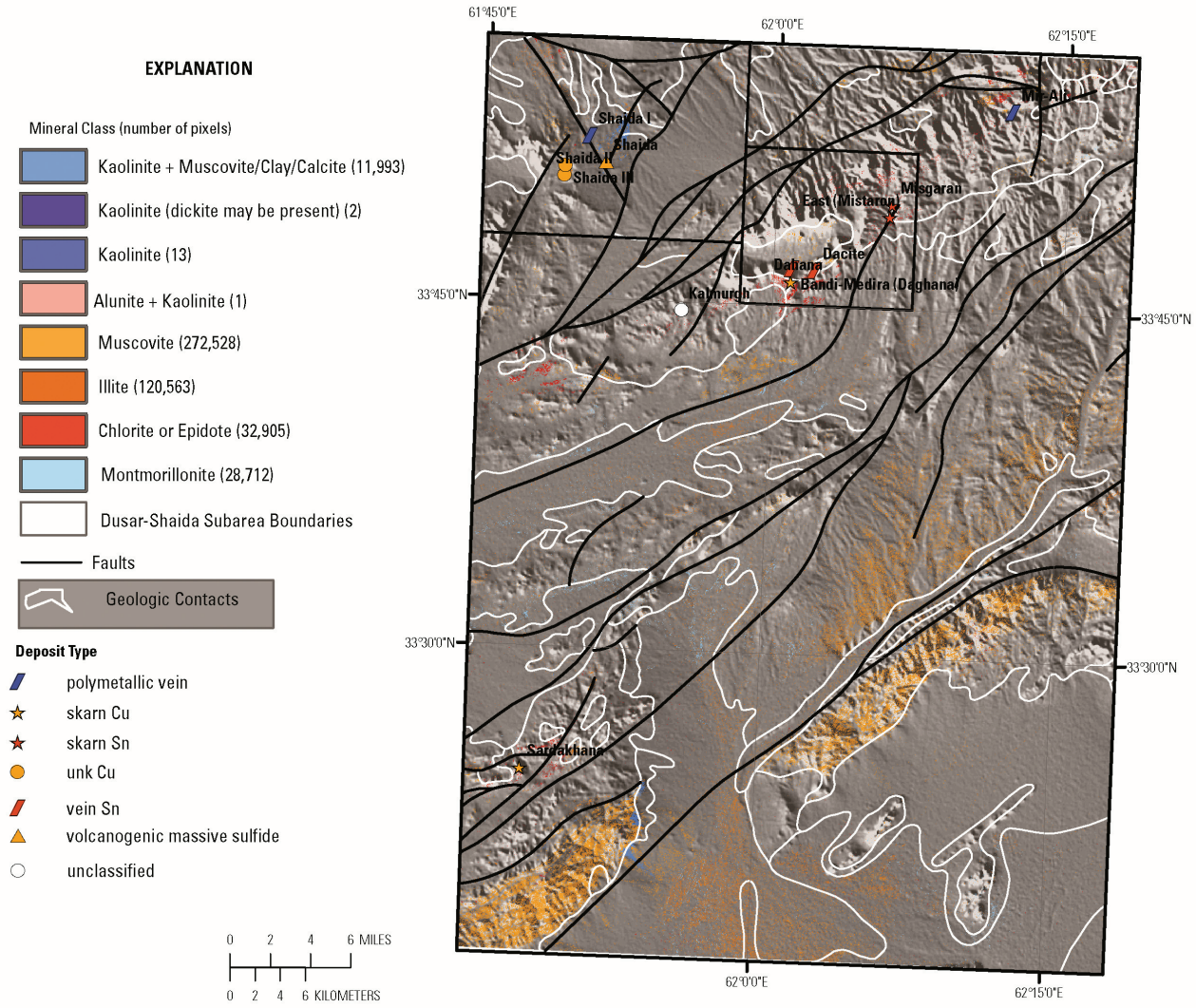

Figure 6B–9. Distribution of clays and micas identified in the HyMap data. Unk, unknown.

6B.4.1.4 Common Alteration Minerals

Most of the minerals in this group are commonly present in hydrothermally altered rocks associated with epithermal processes. Consequently, where they occur in distinct clusters is of great interest in terms of potential mineral deposits.

The Kalmurgh mineral occurrence has associated chlorite or epidote and Fe-bearing carbonates in the Berriasian–Valanginian age rocks immediately around the site. No other minerals detected by the HyMap data are present in the vicinity of Kalmurgh.

The Eocene–Oligocene rocks (lat 33°34′10.54″N., long 62°12′42.72″E.) contain Fe-bearing carbonates (fig. 6B–12). The pixels are not tightly clustered, but are spatially distributed over the entire

geologic unit. Iron-bearing carbonates are also associated with the linear feature observed in the late Quaternary–Recent rocks near lat 33°23′14.24″N., long 62°15′24.34″E., and are known to be related to the infrastructure at the Shindand Airfield.

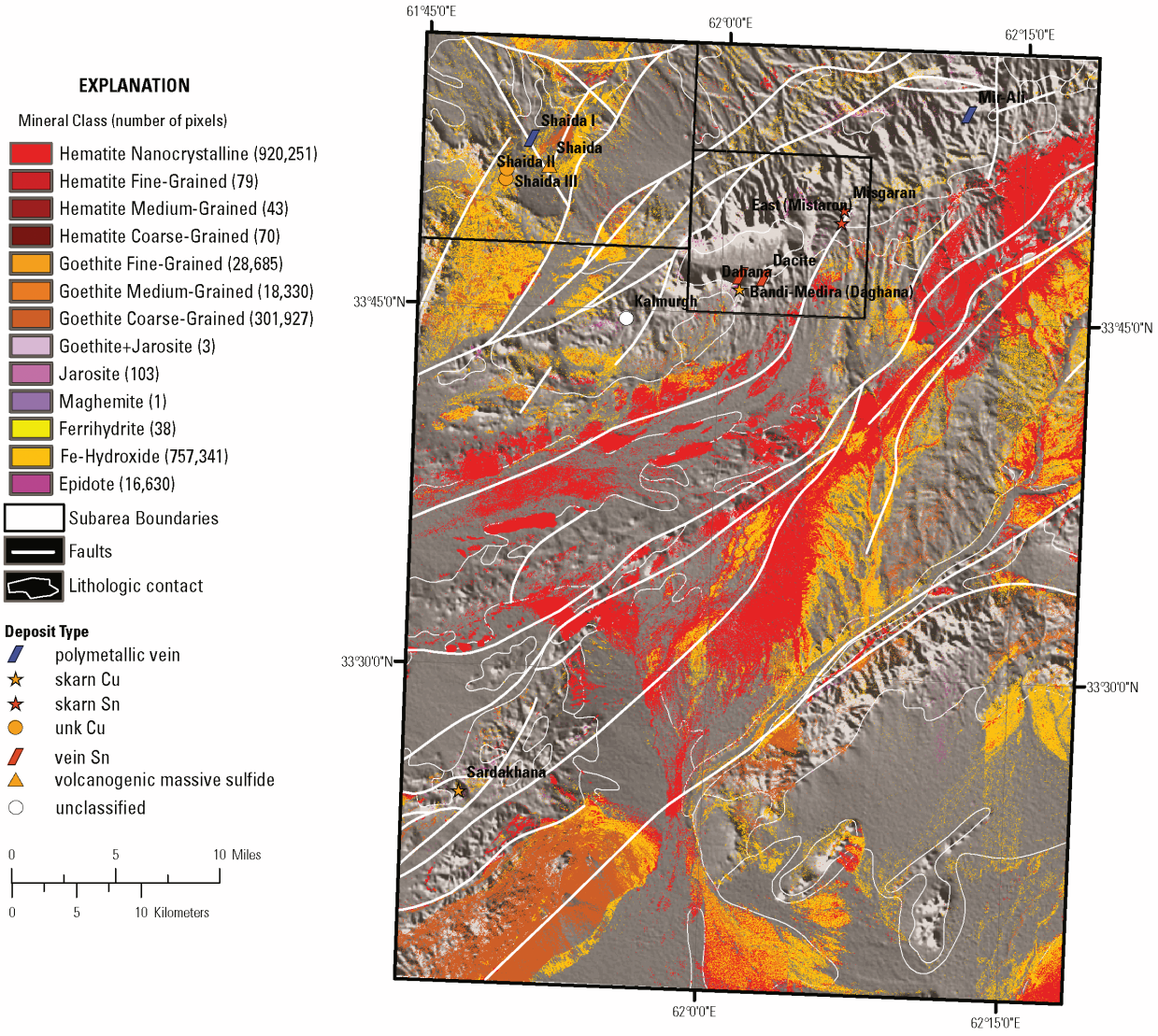

Figure 6B–10. Distribution of Iron-hydroxides and Iron-oxides mapped using the HyMap data for the Dusar-Shaida area of interest. Unk, unknown.

Kaolinite, chlorite or epidote, and Fe-carbonate pixels are present in the Valanginian–Hauterivian rocks on the east side of the AOI. A spatially coherent group of kaolinitic pixels occur along the fault trace that separates the Valanginian–Hauterivian rocks and the sliver of Pliocene rocks (lat 33°30′29.86″N., long 62°7′21.85″E.). In the TM image (fig. 6B–3), these fault-bounded rocks are shown to be dark red-brown and south of the nearby river. A spatially well-defined group of kaolinitic pixels (centered near lat 33°22′51.72″N., long 61°53′44.75″E.) occurs along the geologic contact of the Eocene-Oligocene, Valanginian-Hauterivian, and Pliocene age rocks.

A NE-SW trend (lat 33°42′42.28″N., long 62°0′12.55″E. to lat 33°40′58.76″N., 61°56′58.47″E.) of spatially coherent buddingtonite is present in the Eocene–Oligocene rocks. Abundant buddingtonite and minor amounts of chlorite or epidote and Fe-carbonates are also mapped in the Eocene–Oligocene rocks (lat 33°23′15.94″N., long 62°7′8.54″E.) in the southern part of the area.

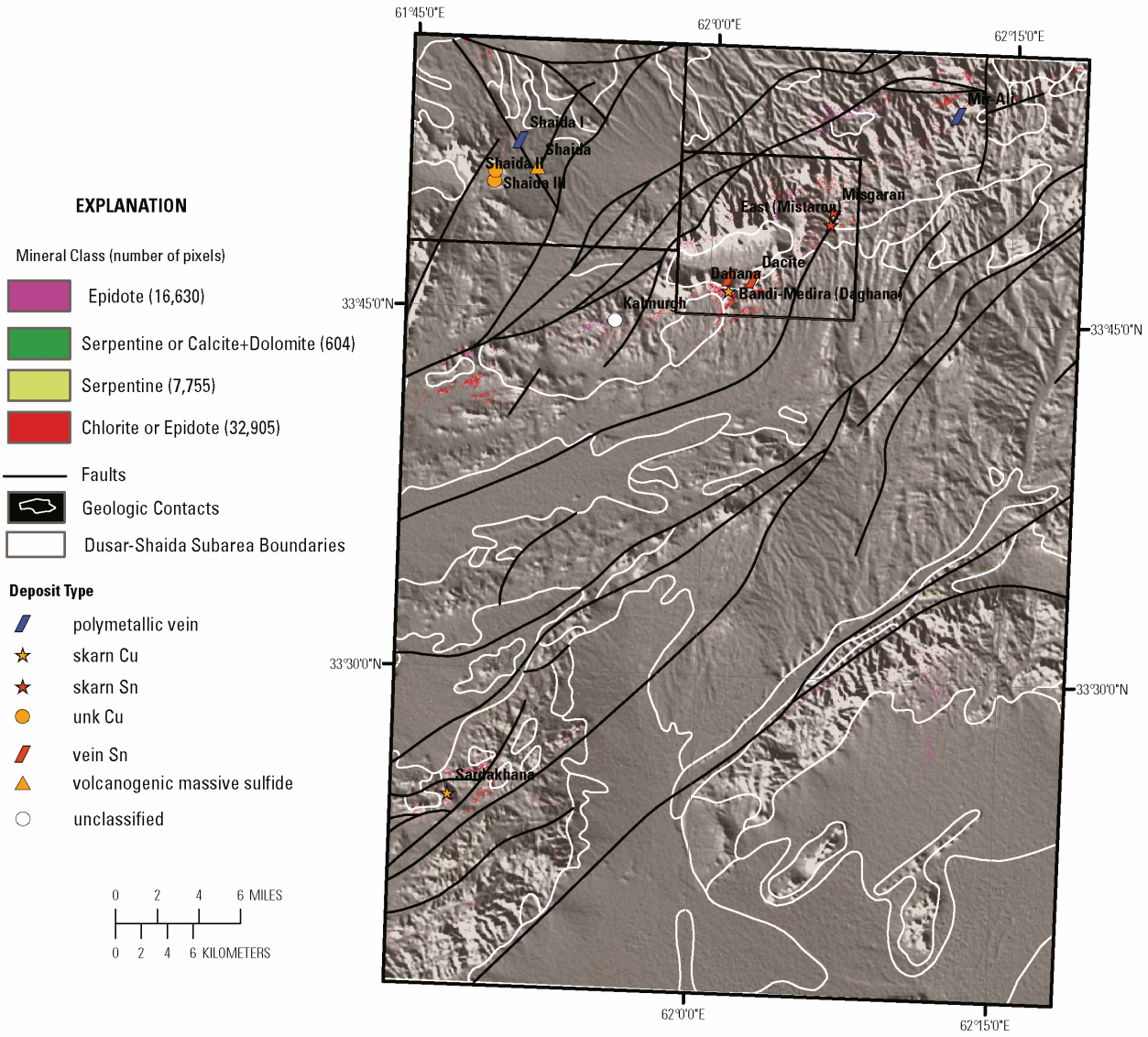

Figure 6B–11. Occurrence and distribution of common secondary minerals detected in the HyMap data for the Dusar-Shaida area of interest. Unk, unknown.

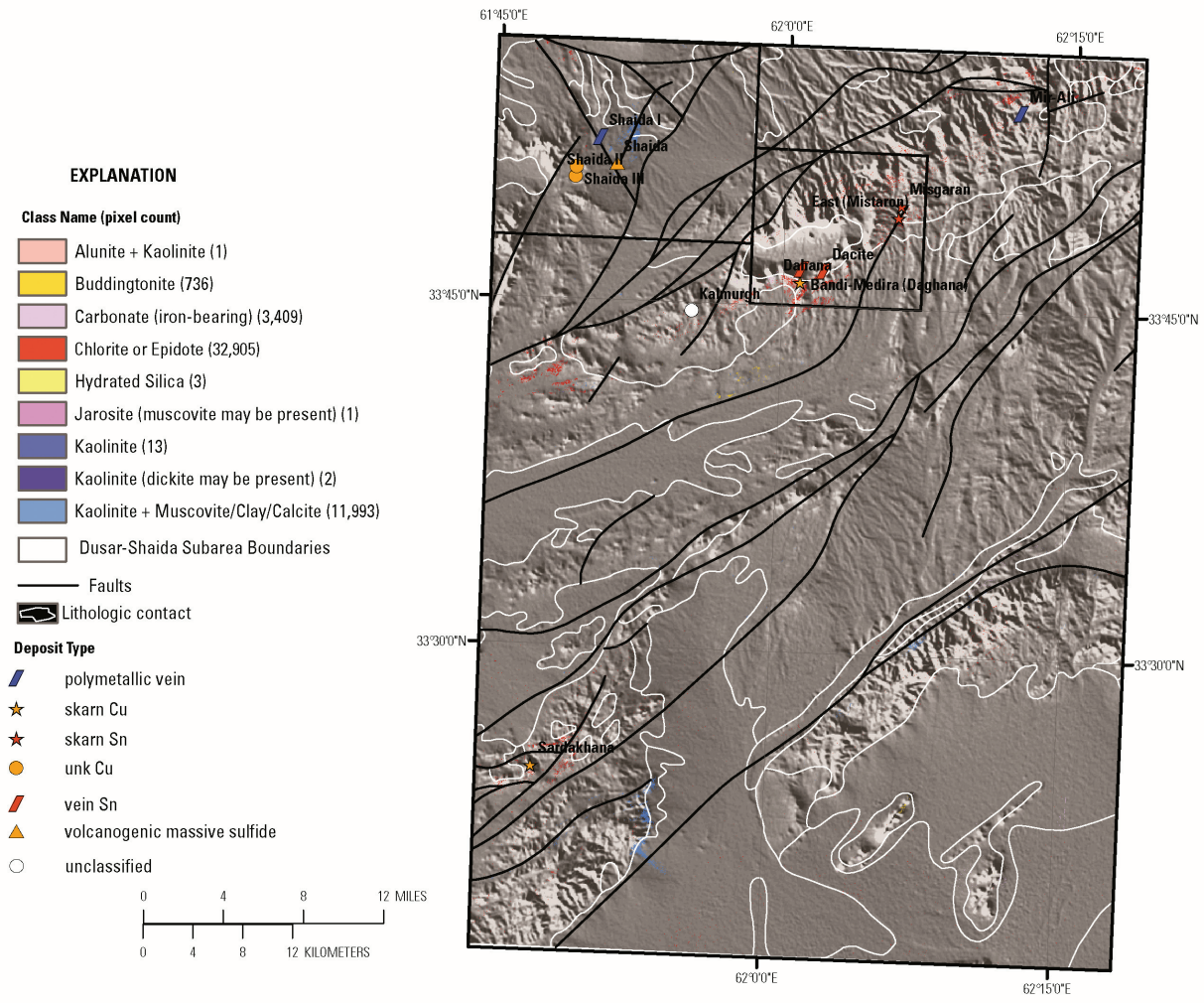

Figure 6B–12. Distribution of common alteration minerals in the Dusar-Shaida area of interest. Unk, unknown.

6B.4.2 Shaida Subarea

The known mineral occurrence map (semi-transparent geologic map overlain on a shaded relief image) shows the position of reported mineral occurrences in Shaida subarea (fig. 6B–13). The subarea is approximately 334 km^2 in size and the topography ranges from 1,099 to 1,578 m (fig. 6B–14).

The colors of the rocks in the TM data (fig. 6B–15) range from light to dark gray, and shades of red, green, and blue. In general, the colors in the TM image do not correlate with the mapped geological units (Doebrich and others, 2006; Dronov and others,1972). The geologic map of the area (fig. 6B–16) shows rocks ranging in age from Late Jurassic to Recent. Early Cretaceous and Oligocene intrusive rocks occur in the central part of the subarea.

Figures 6B–17 shows the distribution of Fe-bearing minerals and 6B–18 shows the distribution of carbonate, sulphate, phyllosilicate, and other alteration minerals. The map of Fe-bearing minerals (fig. 6B–17) shows that pixels of Fe-hydroxide minerals are the most abundant mineral phase in the subarea, followed by Fe^{3+}, Type 1; goethitic; and hematitic minerals. Fewer pixels of Fe^{2+} Fe^{3+}, Type 2; jarosite; and epidote are mapped in the subarea than in the overall AOI.

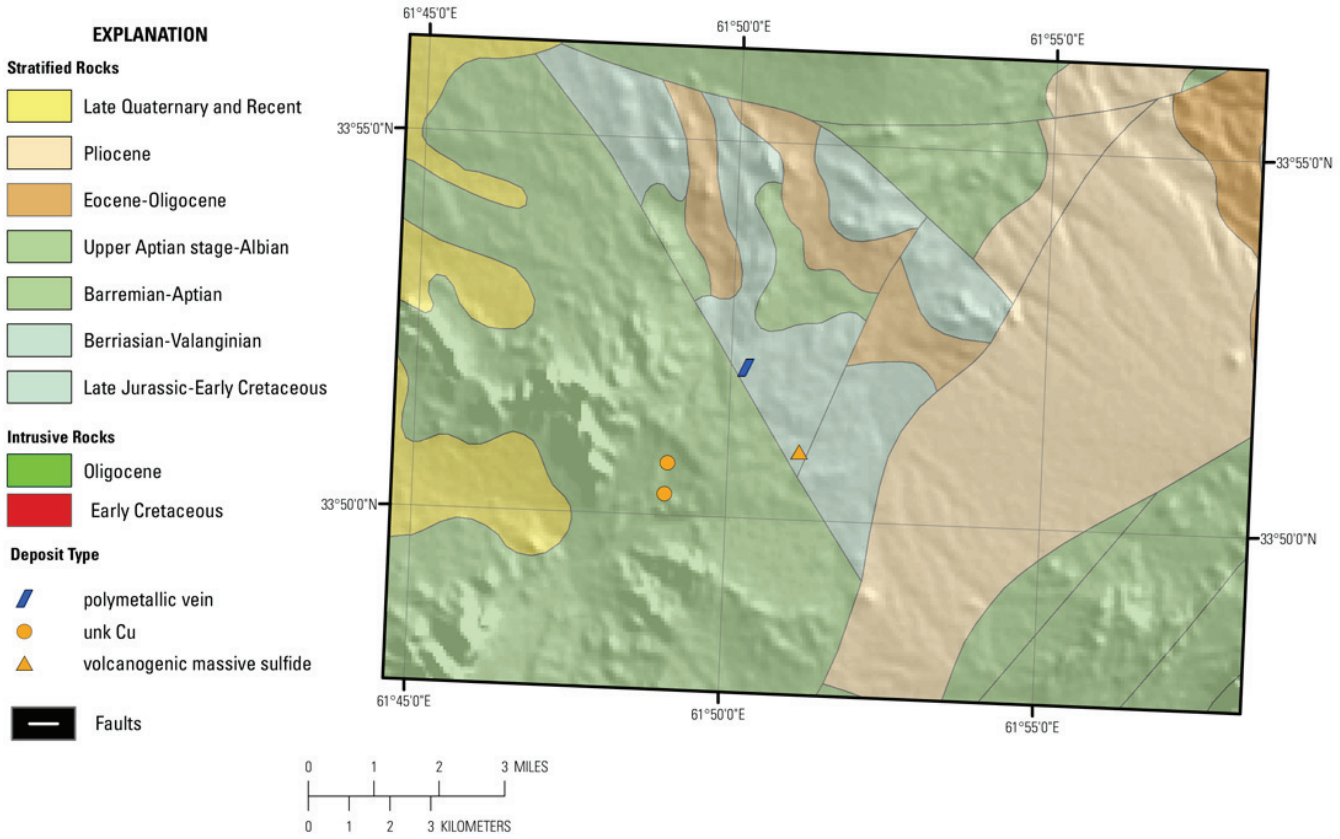

Figure 6B–13 (on previous page). Map showing known mineral occurrences in the Shaida subarea. Unk, unknown.

Figure 6B–18 shows the distribution of carbonates, phyllosilicates, sulphates, altered minerals, and other materials for the subarea. Pixels of calcite and calcite mineral mixtures are pervasive in the area. Although smaller, mineralogically significant and spatially distinct pixels of kaolinite, illite, and muscovite are also mapped. Chlorite or epidote group minerals are detected in small spatially distinct patterns in the western half of the subarea.

The gray to black stripe on the western margin of the maps marks the westernmost boundary of the HyMap dataset.

6B.4.2.1 Shaida Subarea: Carbonate Minerals

Calcite-rich rocks are widespread and occur over the entire subarea (fig.6B–19). A lesser number of pixels of dolomitic mineral mixtures are distributed over much of the area and show no correlation with the mapped geology.

The Shaida and Shaida I prospects are located in regions dominated by calcite + montmorillonite group mineral mixtures. The Shaida II and Shaida III prospects occur in areas with both calcite + muscovite/illite and calcite + montmorillonite mineral mixtures. A few dolomite pixels are spatially scattered over the subarea.

6B.4.2.2 Shaida Subarea: Clays and Micas

The HyMap data (fig. 6B–20) shows the enrichment of clays and micas in the Shaida subarea. Kaolinitic mineral mixtures, muscovites, and illites are the spatially dominant mineral groups. The muscovites and illites preferentially occur in the Eocene–Oligocene and older geologic units.

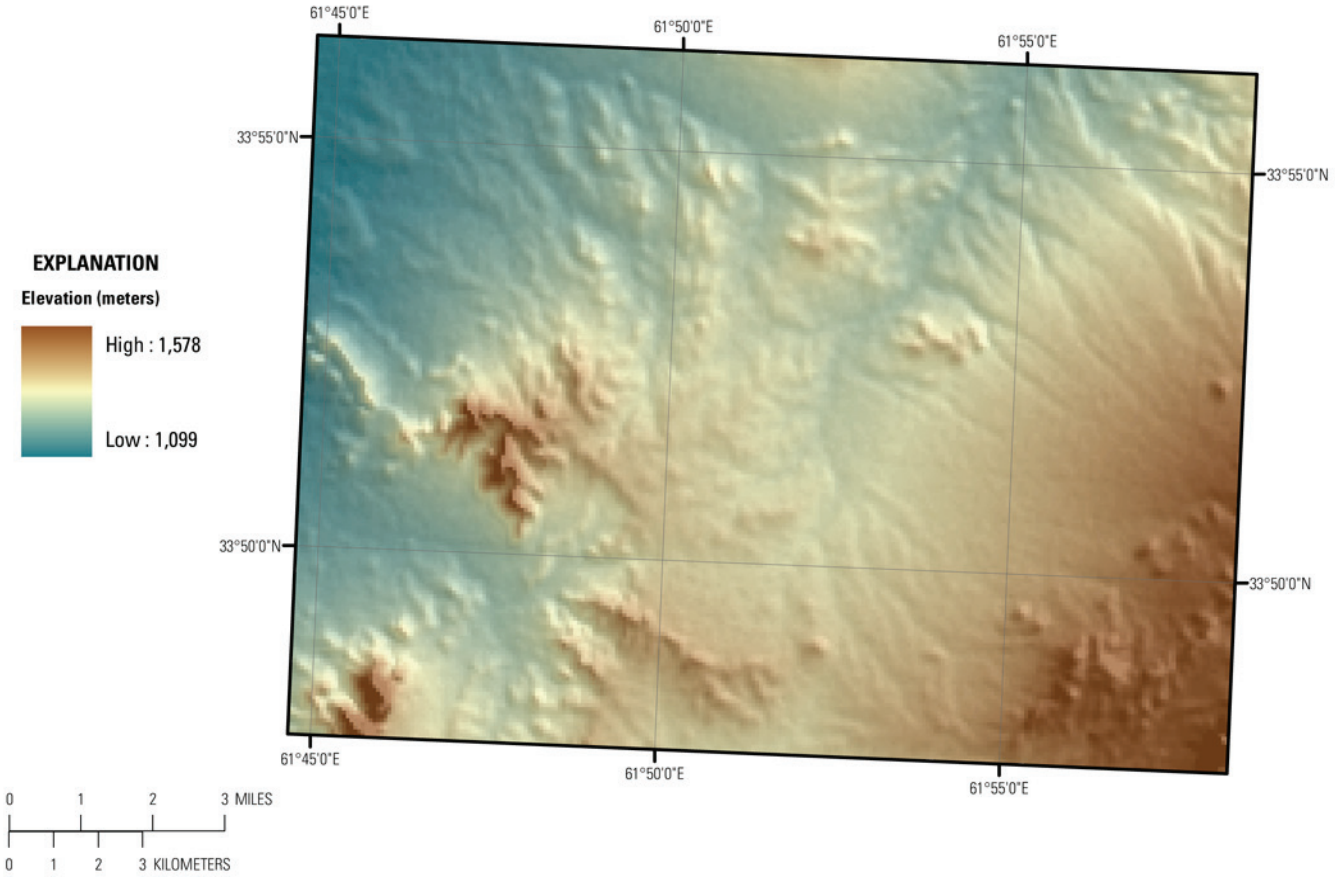

Figure 6B–14. Shaded relief map showing elevation in the Shaida subarea. The darker brown tones indicate higher elevations and lower elevations are represented by the blue tones.

The chlorite or epidote mineral group is spatially most consistent in the Berriasian–Valanginian and Upper Jurassic–Lower Cretaceous (northwest corner of the subarea) rocks where it is associated with illites and muscovites.

A spatially coherent pattern of kaolinite-rich material occurs along the northeast-trending fault trace originating near the Shaida volcanogenic massive sulfide site. This coherent grouping of kaolinitic pixels occurs, along with illite and muscovite group minerals, in Late Jurassic–Early Cretaceous, Early Cretaceous, and Oligocene age rocks.

6B.4.2.3 Shaida Subarea: Iron-Oxide and Iron-Hydroxide Minerals

Figure 6B–21 shows the distribution of Fe-oxides and Fe-hydroxides in the Shaida subarea. The Fe-hydroxide mineral group is the spatially dominant mineral group.

Hematite group minerals are widely distributed over the subarea. However, a spatially consistent group of hematite is mapped on the fringe of a large alluvial fan (lat 33°54′50.72″N., long 61°52′25.61″E.) that intersects Oligocene, Barremian–Aptian, and Late Jurassic–Early Cretaceous age rocks.

Epidote pixels are detected in the Berriasian–Valanginian rocks in the extreme southeast corner of the subarea (lat 33°47′58.18″N., long 61°58′13.81″E.).

Spatially consistent patterns of goethitic minerals are distributed over the subarea. Additional moderate size concentrations are present along the western margin of the large alluvial fan (lat 33°55′3.62″N., long 61°50′49.79″E.) in the Berriasian–Valanginian and late Quaternary–Recent rocks. The largest and most coherent group of goethite pixels occurs along the northeast-trending fault trace

originating near the Shaida site in Late Jurassic–Early Cretaceous, Early Cretaceous, and Oligocene age rocks (King, Johnson, and others, 2011).

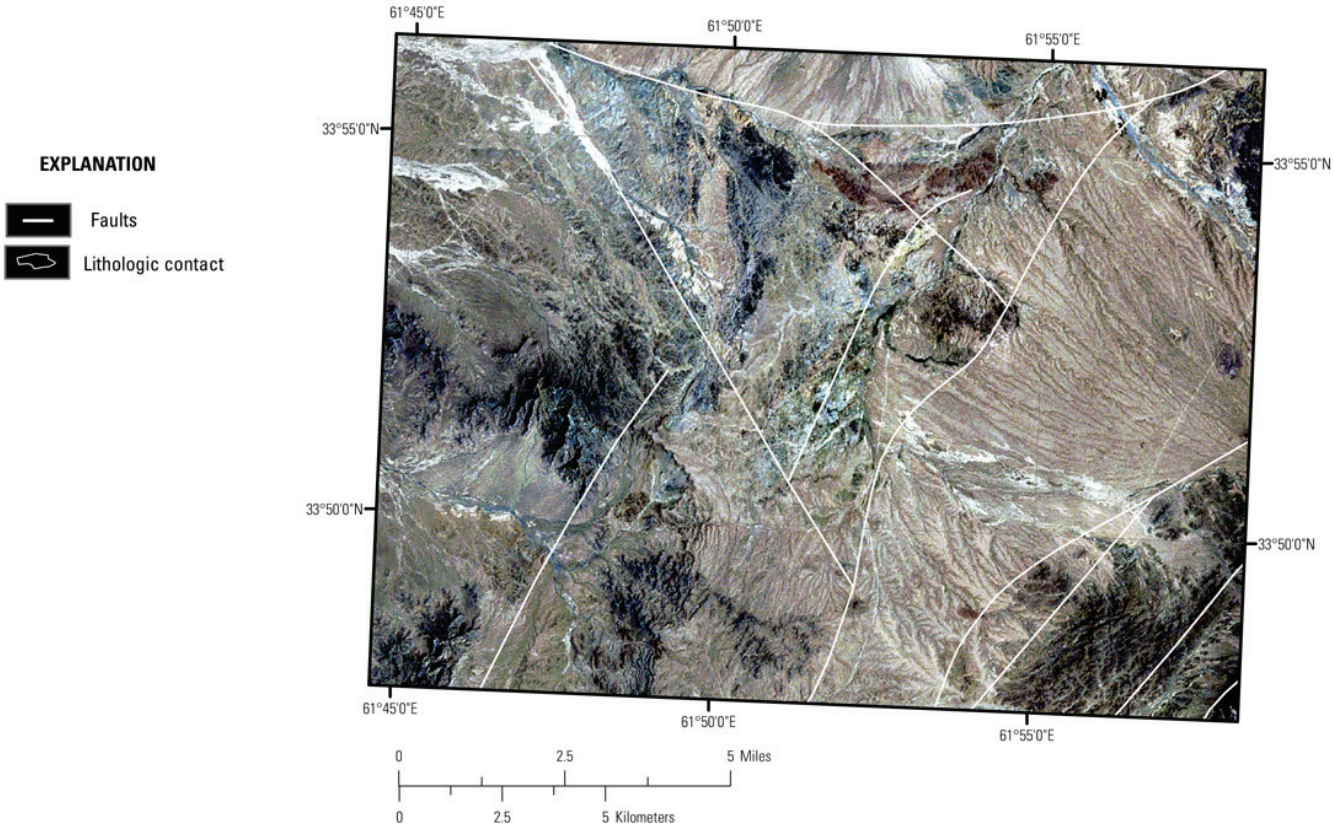

Figure 6B–15. Landsat Thematic Mapper image showing the numerous faults and fractures of different orientations and extent that are present in the Shaida subarea.

6B.4.2.4 Shaida Subarea: Common Secondary Minerals

The epidote and chlorite or epidote mineral groups are the most abundant secondary minerals (fig. 6B–22) in the subarea. The largest concentration of these pixels occurs in the Barriasian–Valanginian rocks in the southeast corner of the subarea and in the Upper Jurassic–Lower Cretaceous rocks in the northwest part of the subarea. Chlorite or epidote group minerals are also present near the Shaida II and Shaida III prospects in Barriasian–Valanginian host rocks. Serpentine and serpentine mineral mixtures are few and are spatially scattered over the subarea.

6B.4.2.5 Shaida Subarea: Common Alteration Minerals

Kaolinite group minerals are the spatially most abundant common alteration products detected in the HyMap data (fig. 6B–23). A spatially extensive group of kaolinite is mapped near lat 33°52′12.76″N., long 61°52′4.65″E. on either side of a generally northeast-trending fault that terminates near the Shaida occurrence in Late Jurassic–Early Cretaceous, Early Cretaceous, and Oligocene age rocks. Chlorite or epidote minerals are detected and mapped in the Barriasian–Valanginian rocks (southeast corner) and in the Late Jurassic–Early Cretaceous age rocks (northwest part) of the subarea. Minor amounts of chlorite are distributed over the subarea with some spatially coherent patterns in the Eocene–Oligocene rocks in the northeast corner of the subarea. The Fe-bearing carbonates are spatially widely distributed over the southeast part of the subarea. A small, but spatially coherent group of buddingtonite is mapped near lat 33°55′2.813″N., long 61°56′59.11″E. in undifferentiated Pliocene rocks (see King, Johnson, and others, 2011).

6B.4.3 Dahana-Misgaran Subarea

The known mineral occurrence map shows the position of the five reported sites of mineralization in the Dahana-Misgaran subarea (fig. 6B–24). The topography in the area ranges from 1,340 to 1,949 m (fig. 6B–25), and the geologic age of the rocks range from Berriasian-Valanginian to late Quaternary (fig. 6B–26; Doebrich and others, 2006; Dronov and others, 1972).

In the Landsat TM data (Davis, 2007), the Oligocene intrusive rocks in the west-central part of the subarea are easily recognized by their overall light color (fig. 6B–27). Light-colored rocks in the southwest corner of the subarea are Berriasian–Valanginian age and texturally appear to be surficial weathering products. Darker colored, seemingly bedded, units are present in the north-central portion of the subarea in Berriasian–Valanginian rocks. The five known mineralized locations (Misgaran, East Mistaron, Dacite, Bandi-Medira, and Dahana) occur in stratified rocks of Berriasian–Valanginian or Oligocene intrusive rocks.(fig. 6B–24).

Hyperspectral data for the area (figs. 6B–28 and 6B–29) show the distribution of Fe-bearing minerals, carbonate, phyllosilicate, sulphate, and other alteration minerals, respectively. Several Fe-bearing mineral and minerals groups are present in the Dahana-Misgaran subarea. However, calcite and calcite group minerals spatially dominate the subarea (fig. 6B–29, fig. 6B–30).

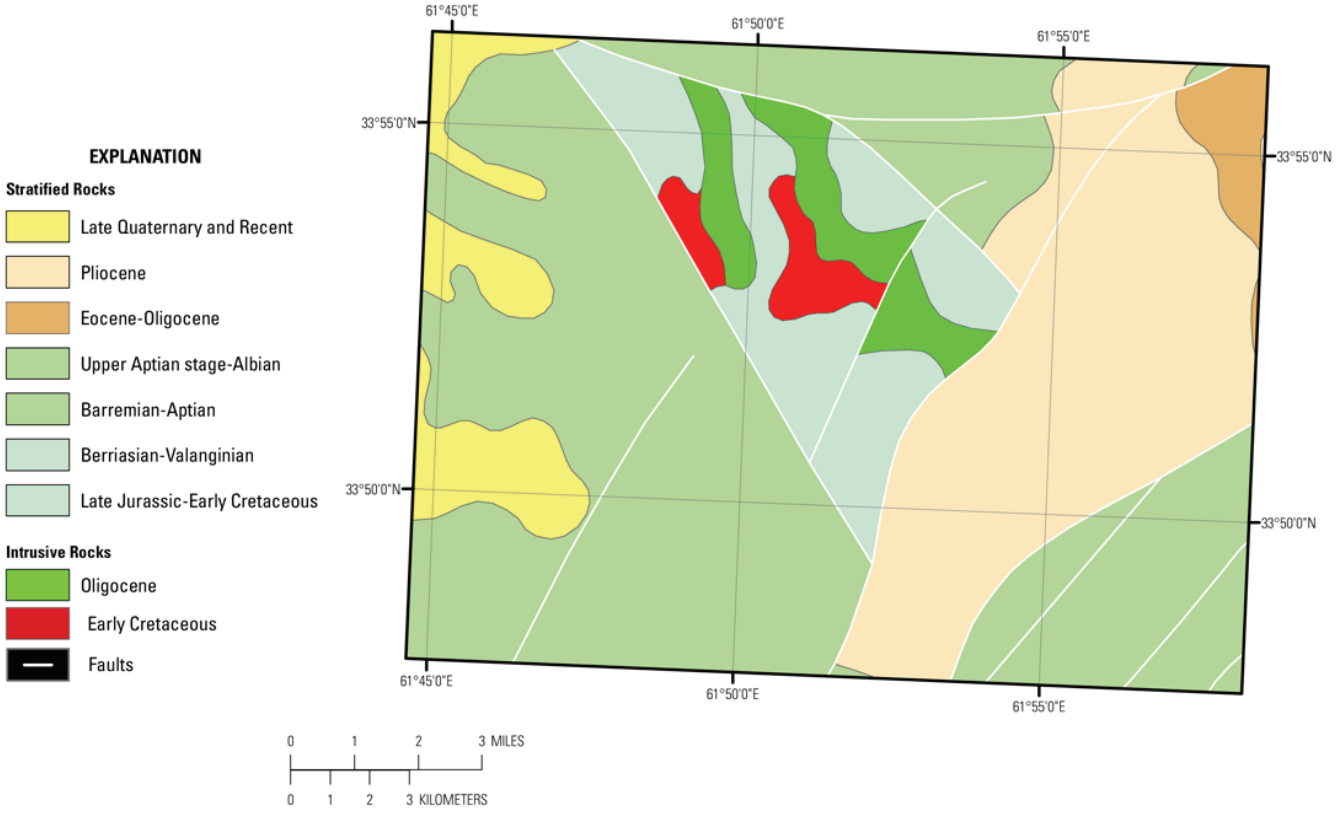

Figure 6B–16. Geologic map of the Shaida subarea derived from Doebrich and others (2006).

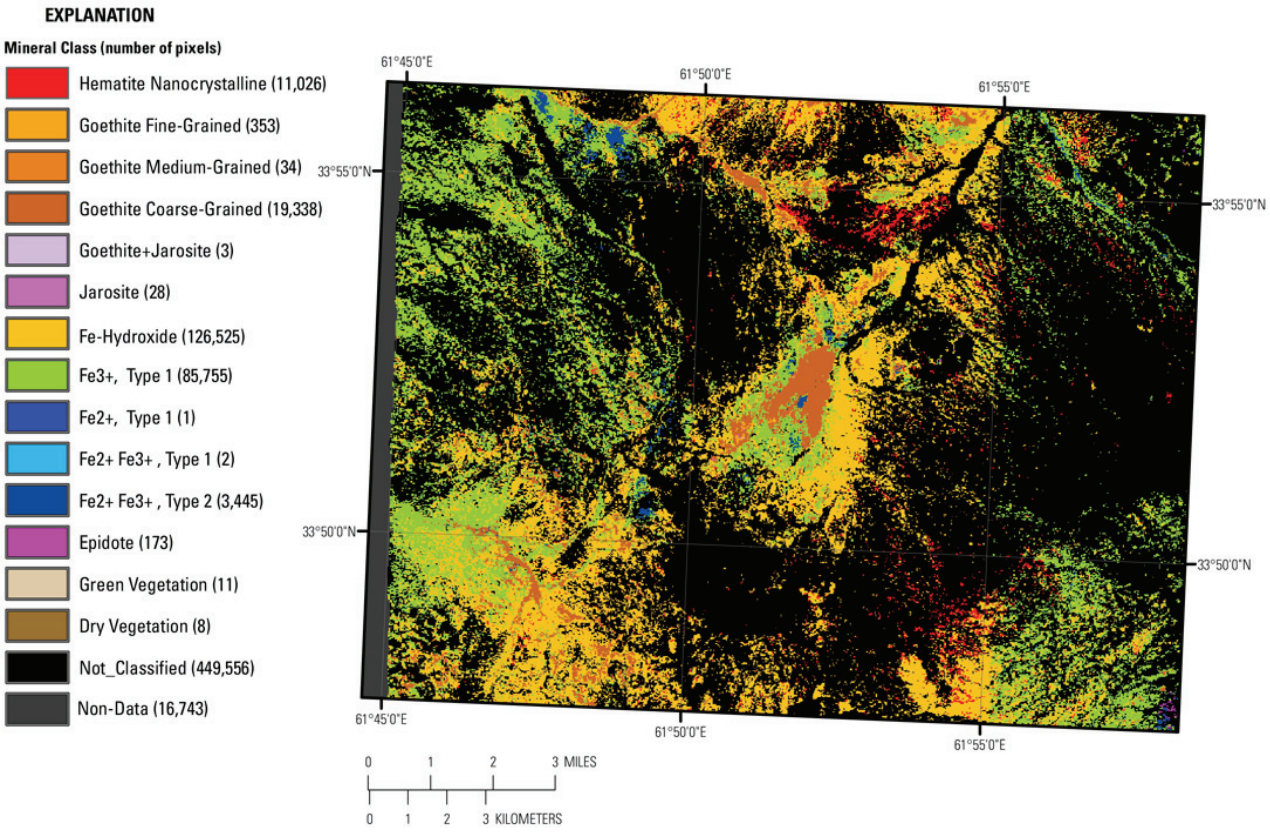

Figure 6B–17. The iron-bearing and alteration minerals detected in the HyMap data for the Shaida subarea are shown in this image.

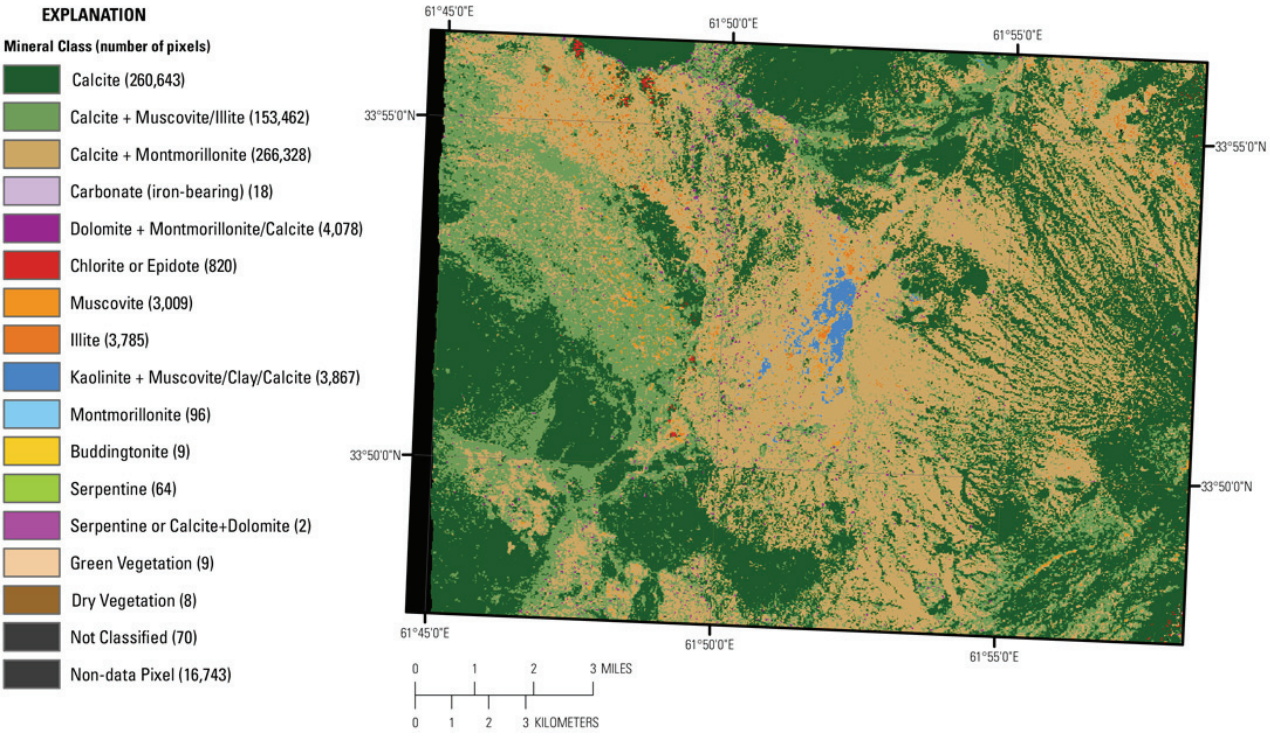

Figure 6B–18. Distribution of clays, carbonates, phyllosilicates, sulphates, and other alteration minerals for the Shaida subarea.

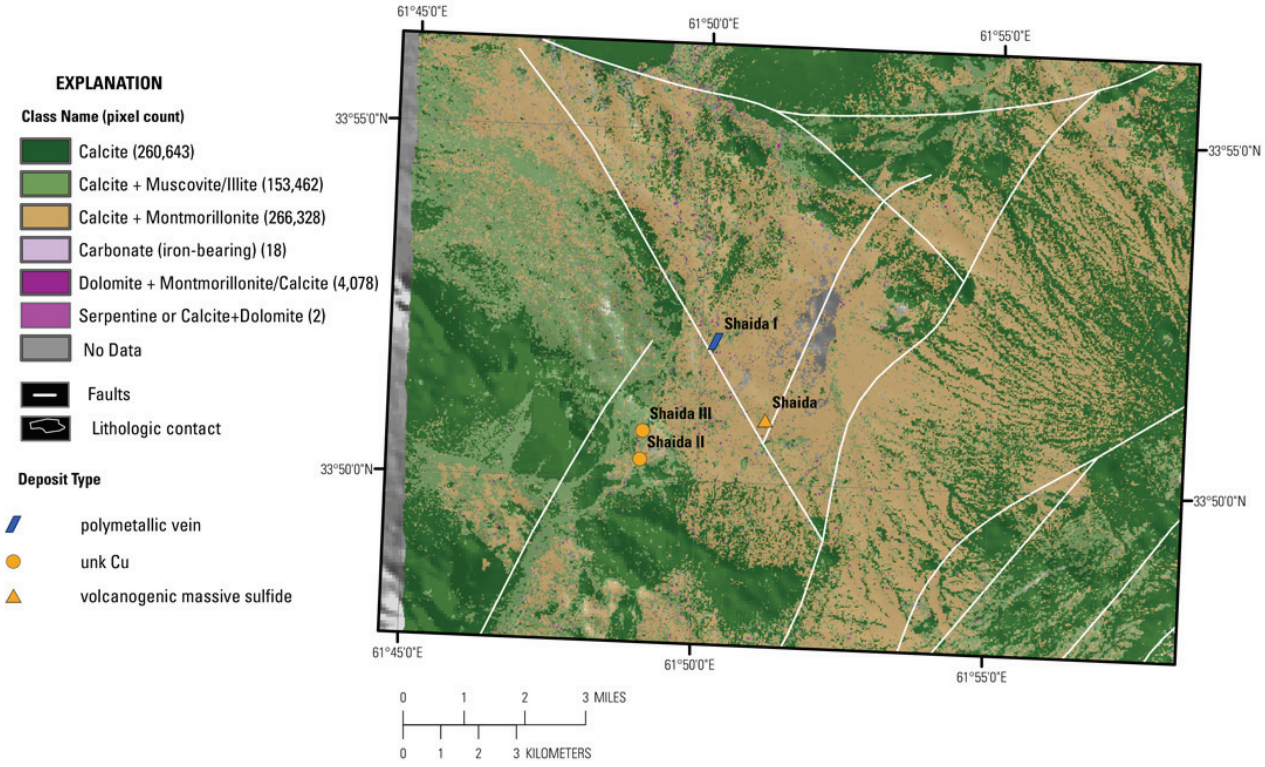

Figure 6B–19. Distribution of carbonate-bearing minerals in the Shaida subarea detected by the HyMap data. Unk, unknown.

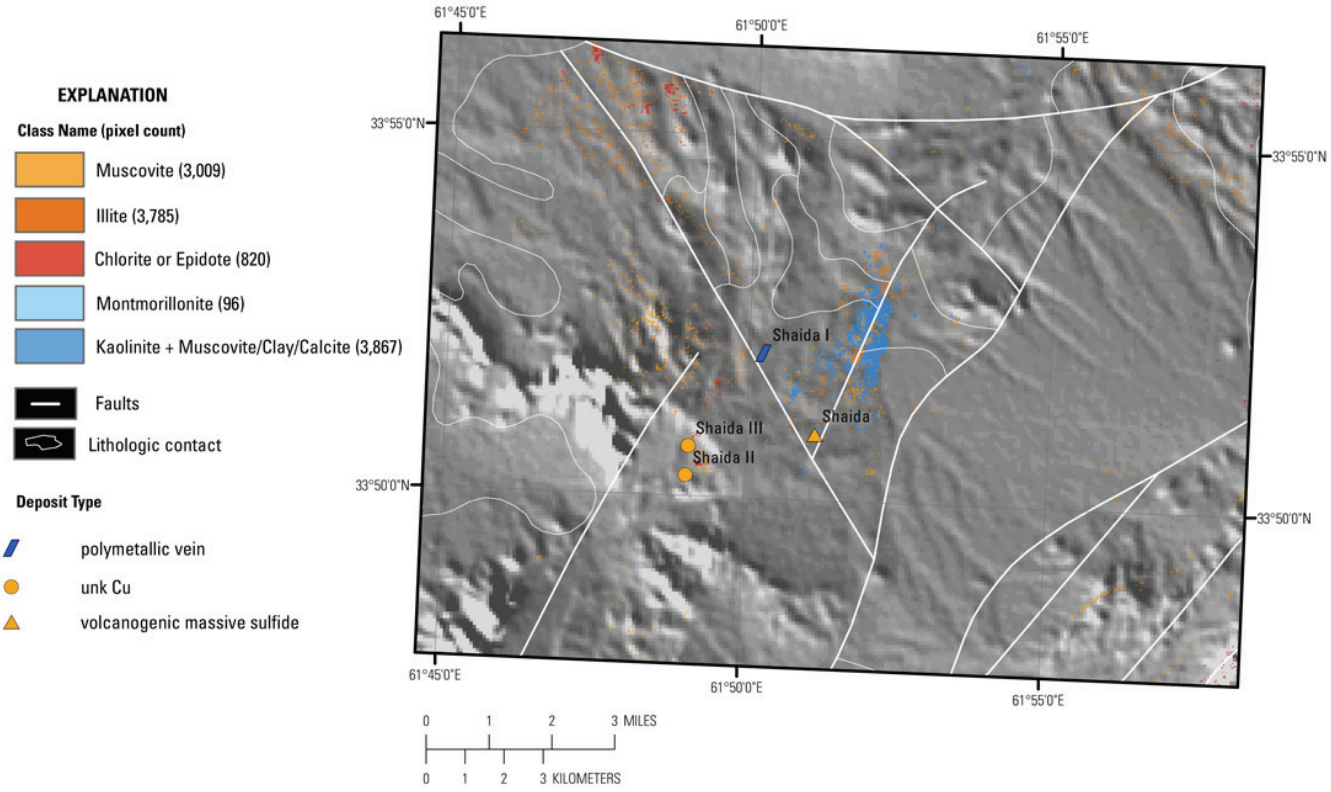

Figure 6B–20. Distribution of clays and micas detected using the HyMap data in the Shaida subarea. Unk, unknown.

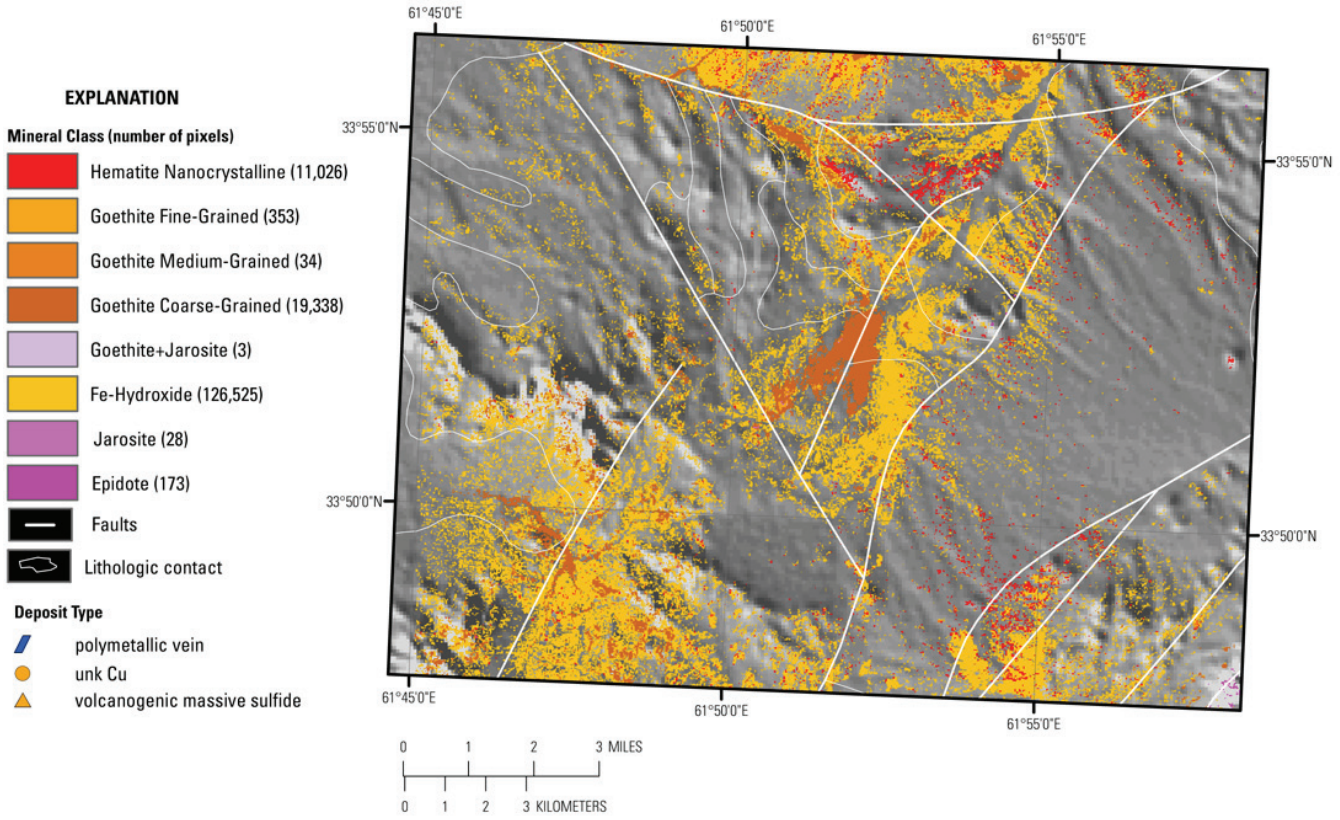

Figure 6B–21. Distribution of Fe-hydroxides and oxides for the Shaida subarea. Unk, unknown.

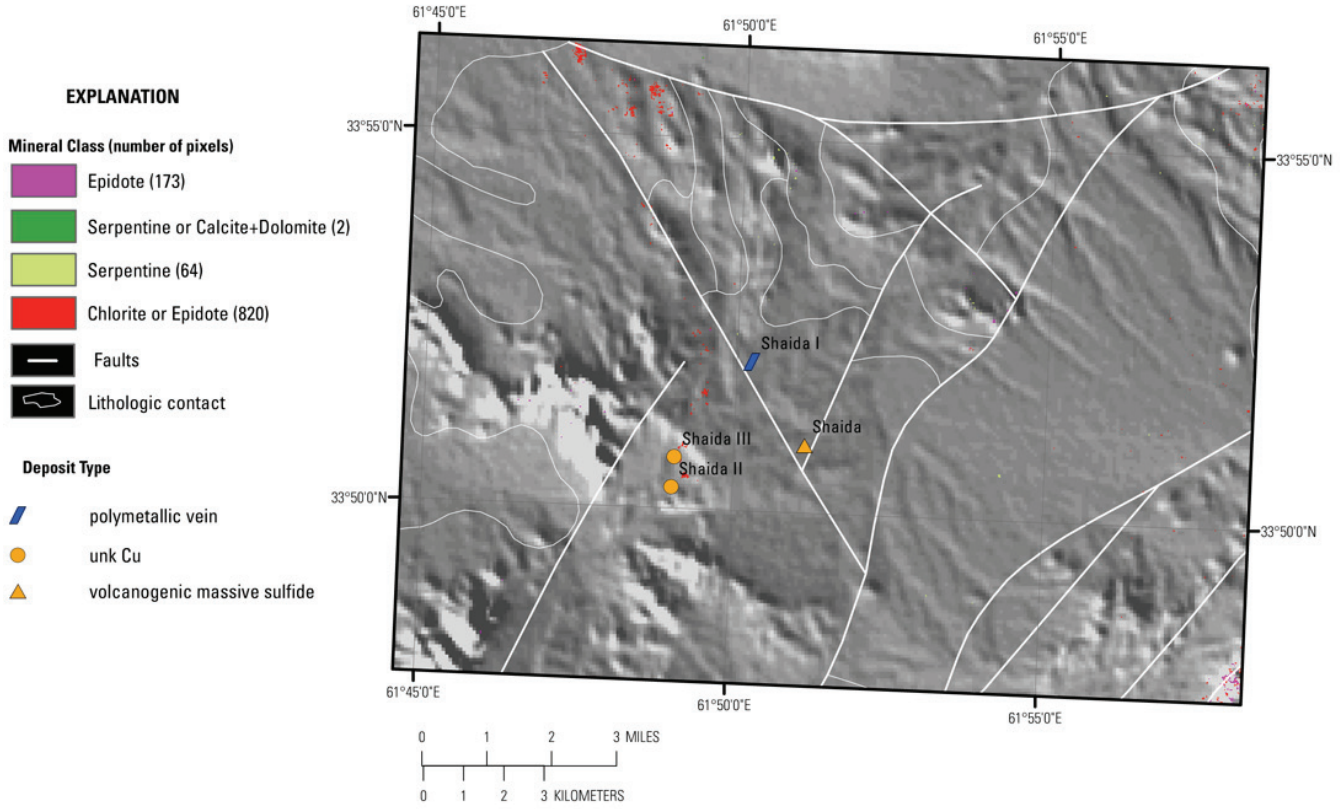

Figure 6B–22. Distribution of common secondary minerals detected in the HyMap data. Unk, unknown.

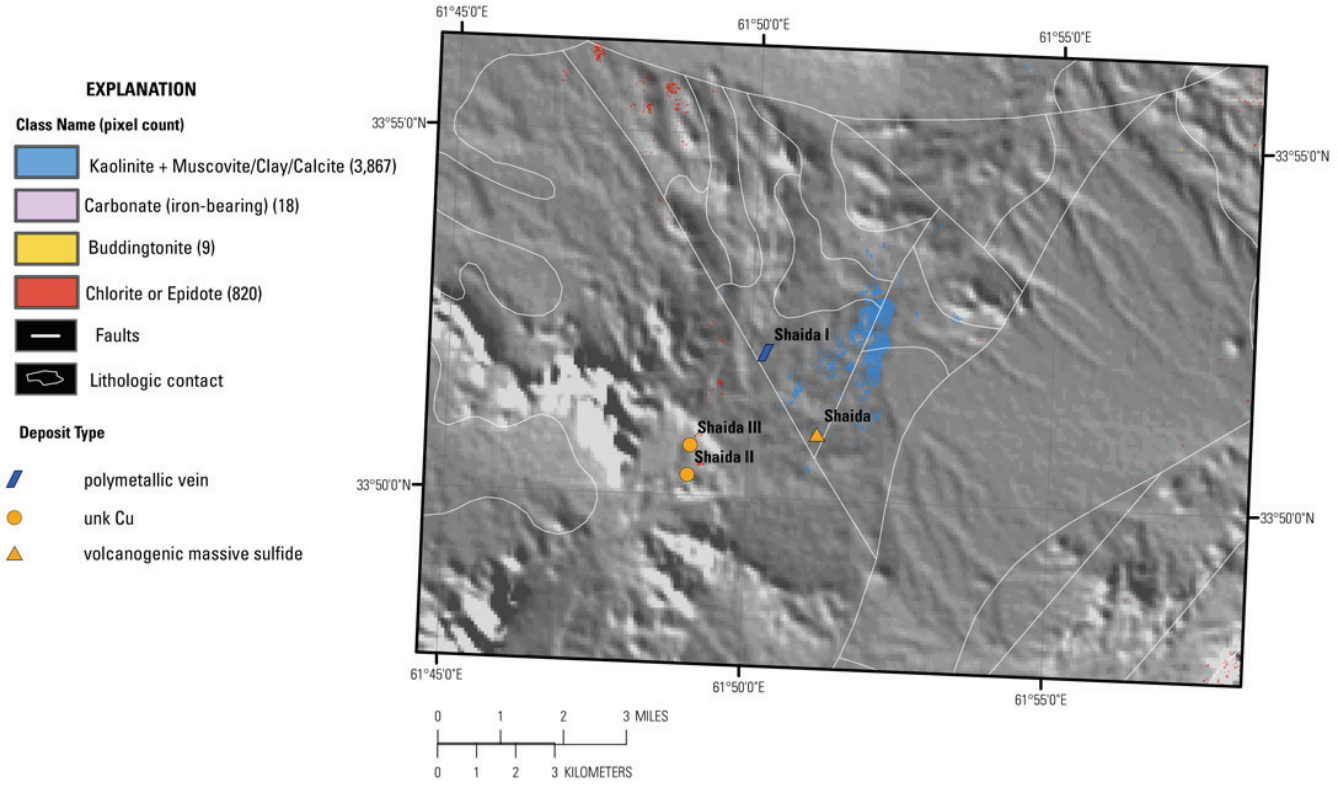

Figure 6B–23. Common alteration materials detected in the HyMap data. Unk, unknown.

6B.4.3.1 Dahana-Misgaran Subarea: Carbonate Minerals

Figure 6B–30 shows wide spatial distribution of carbonate-rich rocks over the entire subarea. Calcite mineral mixtures occur in the northwest and southeast corners of the subarea and are also associated with the Oligocene intrusive rocks. Pixels representative of dolomitic minerals occur in the Oligocene intrusive rocks, but are much less abundant than the pixels of calcite and calcite mineral mixtures. Iron-bearing carbonates occur on the southwest margins of the intrusive unit and in the Berriasian–Valanginian rocks (lat 33°48′59.23″N., long 62°0′37.78″E.) north of the intrusion.

6B.4.3.2 Dahana-Misgaran Subarea: Clays and Micas

Figure 6B–31 shows the enrichment of clays and micas in the Dahana-Misgaran subarea. Chlorite or epidote group minerals are the most abundant phase in the subarea and are primarily associated with intrusive rocks. Although muscovite and illite pixels are mapped throughout the subarea, the largest spatially consistent group of these minerals occurs in the Oligocene intrusive rocks and in the Berriasian–Valanginian rocks south of the mapped intrusive body near the contact with the Eocene-Oligocene unit (fig. 6B–26). The chlorite-epidote minerals primarily occur in the central portion of the subarea in Berriasian–Valanginian and Eocene–Oligocene rocks. Only minor amounts of montmorillonite are mapped in the subarea and occur in the Oligocene intrusive rocks.

6B.4.3.3 Dahana-Misgaran Subarea: Iron Oxides and Hydroxides

The distribution of Fe-oxides and hydroxides is shown in figure 6B–32. Iron-hydroxide minerals are spatially distributed throughout the subarea, with the exception of the Oligocene intrusive rocks. Hematite pixels are spatially present in Pliocene rocks in the southeastern part of the subarea where they occur with Fe-hydroxides. Both hematite and Fe-hydroxide group minerals are present in the late Quaternary and Recent units in the southwest portion of the Dahana-Misgaran subarea. Epidote shows coherent distribution patterns along the margins of the Oligocene intrusion and near the East Mistaron

and Dahana mineral locations. Goethite pixels are primarily mapped in the Eocene–Oligocene and Berriasian–Valanginian (northwest corner of the subarea) rocks.

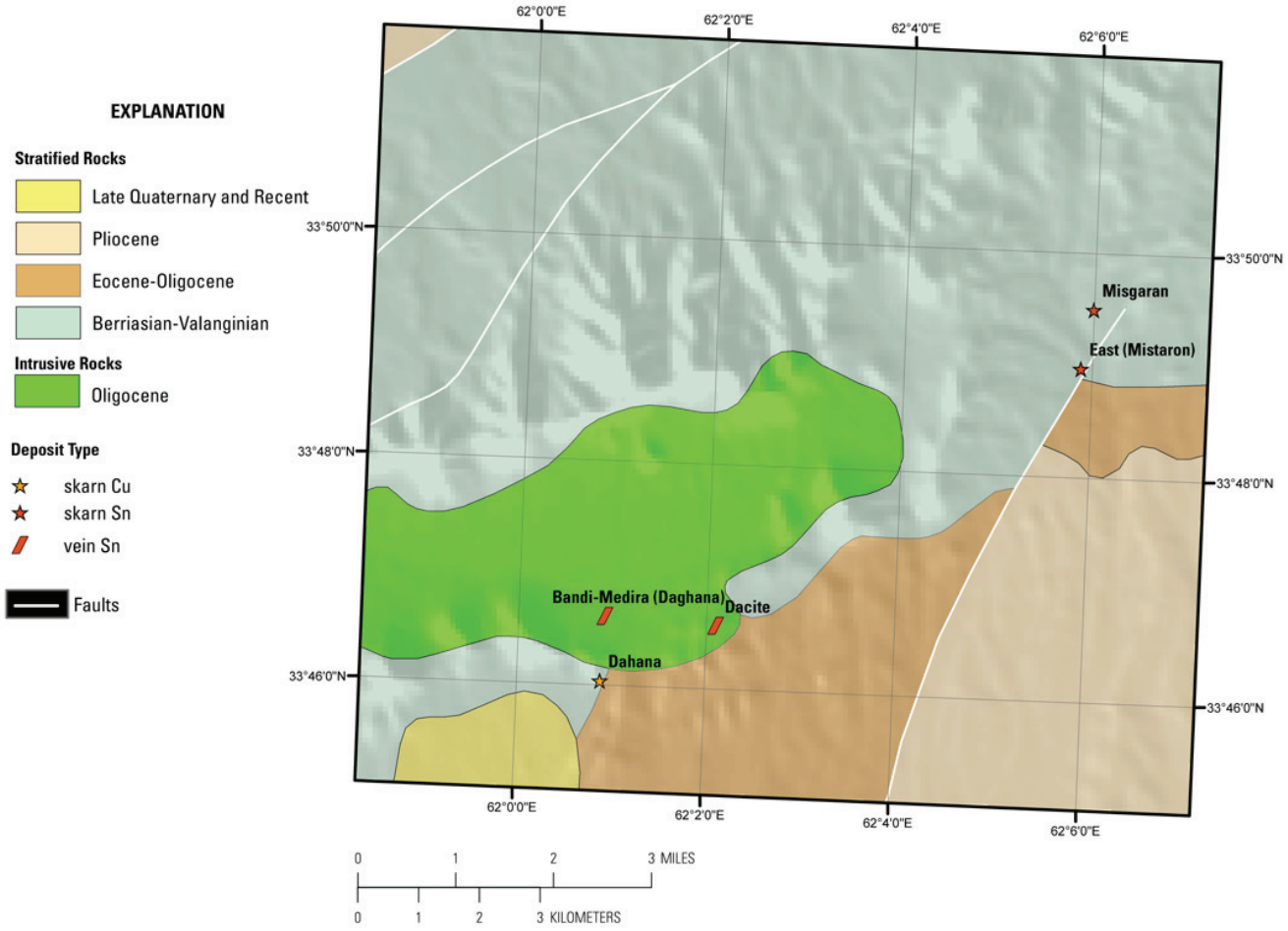

Figure 6B–24. Known mineral occurrences in the Dahana-Misgaran subarea.

6B.4.3.4 Dahana-Misgaran Subarea: Common Secondary Minerals

There are few occurrence of common secondary minerals (fig. 6B–33), with exception of the chlorite or epidote, and epidote groups. Pixels of chlorite and epidote are present in the Berriasian-Valanginian and Eocene–Oligocene rocks that surround the Oligocene intrusion. These minerals form a spatially consistent pattern on the outer margins of the intrusion. Both chlorites and epidotes are present near the Dahana and East Mistaron prospects.

Serpentine minerals are not spatially abundant and show no significant patterns of concentrations with a only slight increase in the number of pixels in the Berriasian–Valanginian rocks in the southwest corner of the subarea.

6B.4.3.5 Dahana-Misgaran Subarea: Common Alteration Minerals

The only significant coherent spatial distribution pattern in the common alteration group minerals are the chlorite or epidote group and the Fe-bearing carbonates (fig. 6B–34). The Fe-bearing carbonates favor the Berriasian–Valanginian unit (southwest corner of the subarea). The chlorite or epidote group also occurs preferentially in the Berriasian–Valanginian rocks with some presence in the Eocene–Oligocene unit (lat 33°46′8.37″N., long 62°2′25.86″E.).

As previously mentioned the chlorite or epidote group show spatially coherent patterns near the mineralized Dahana and East Mistaron mineralized locations.

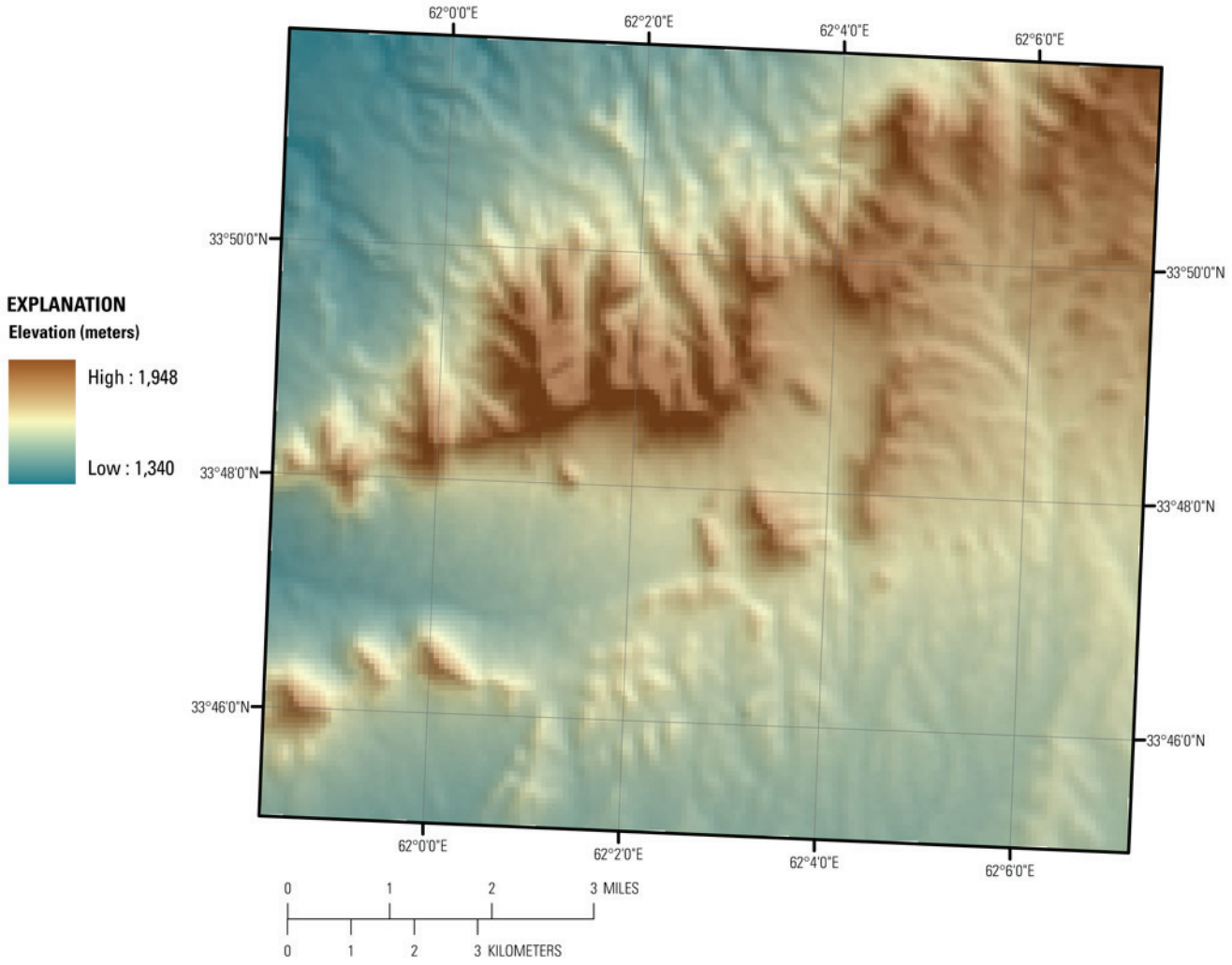

Figure 6B–25. Shaded relief map showing elevation of the Dahana-Misgaran subarea. The darker brown tones indicate the higher elevations and the lower elevations are represented by the blue tones.

6B.5 Summary and Conclusions

The HyMap data for the Dusar-Shaida AOI suggest several locations that warrant additional field sampling as well as geophysical and geochemical characterization. Differences between the current geological map and the spatial distribution patterns of minerals and minerals groups in the HyMap data, as well as the color and textural character of the Landsat TM data, suggest that the current geologic map should be reevaluated to ensure accuracy of ages of geologic units and known fault traces in the AOI.

The HyMap data indicate that the Dusar-Shaida AOI has a high potential for yielding new prospects of mineralization. The presence of kaolinites is frequently associated with hydrothermal processes. Detection of kaolinites is of increased interest if they are associated with faulting (pathways for fluid flow) and (or) exhibit well-defined spatial distribution patterns (which may be indicative of structural control). A well-defined cluster of kaolinite, goethite, and Fe-hydroxide material centered near lat 33°22′51.72″N., long 61°53′44.75″E. occurs along the geologic contact of the Eocene–Oligocene, Valanginian–Hauterivian, and Pliocene age rocks. Heat associated with the intrusive rock formation/emplacement may have mobilized hydrothermal fluids along the geologic contacts, which in turn produced mineralized rocks. This combination of minerals and their close proximity to the Eocene-Oligocene intrusion makes the region ideal for additional geochemical and geophysical analysis.

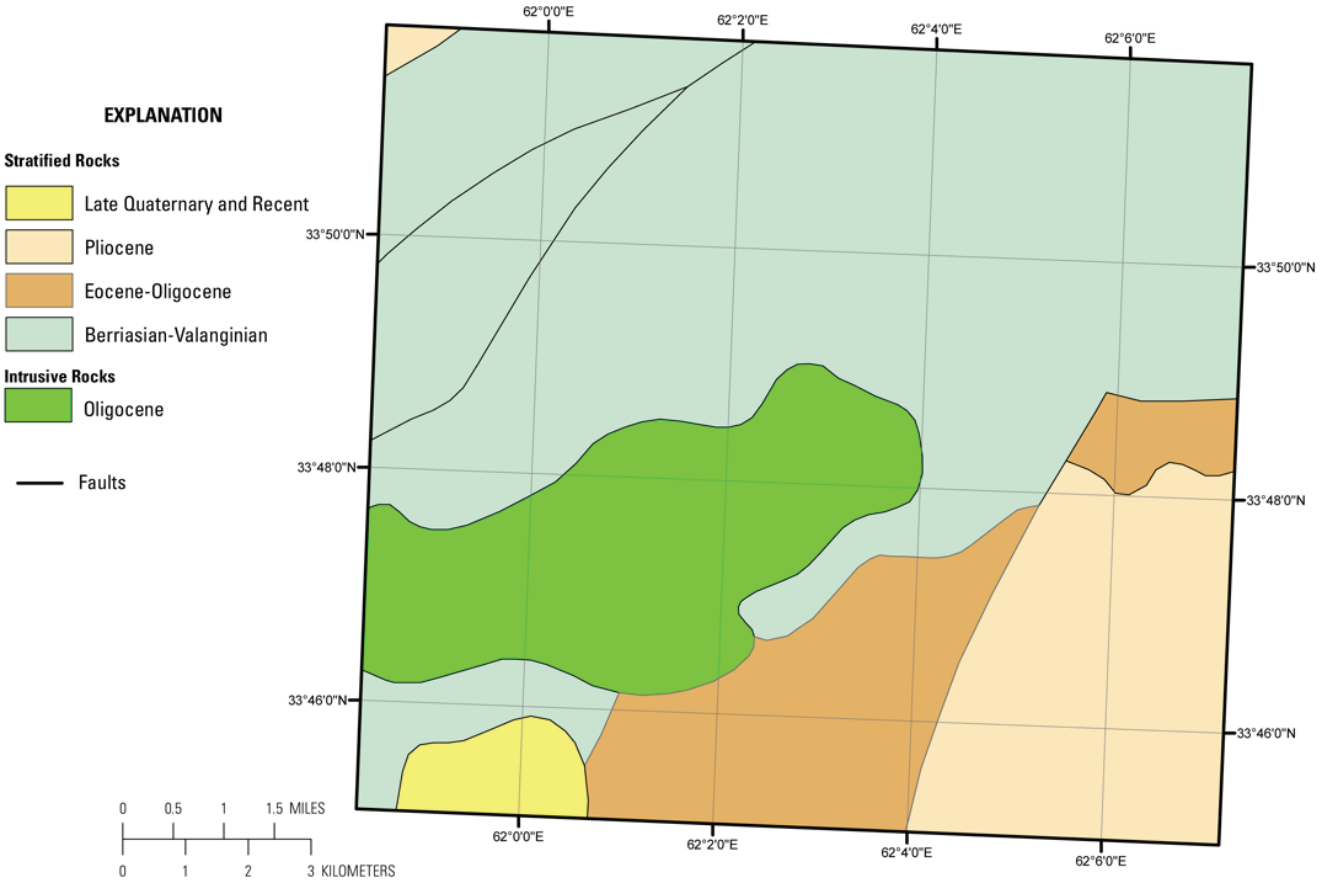

Figure 6B–26. Geologic map of the Dahana-Misgaran subarea is taken from Doebrich and others (2006).

A spatially coherent group of kaolinite, goethite, and Fe-hydroxide minerals also occurs along a fault separating Pliocene and Valanginian–Hauterivian age rocks (lat 33°30′29.86″N., long 62°7′21.85″E.). Although lacking a nearby intrusive body, this occurrence warrants additional field verification.

A northeast-southwest trend (lat 33°42′42.28″N., long 62°0′12.55″E. to lat 33°40′58.76″N., long 61°56′58.47″E.) of buddingtonite is present in the Eocene–Oligocene rocks in the western half of the AOI. The buddingtonite is associated with montmorillonite, illites, hematite, goethites, and Fe-hydroxyl minerals. Its close proximity to a fault increases the potential for ore-body formation as the fault may serve as a conduit for the movement of fluids associated with epithermal mineralization.

Abundant buddingtonite and minor amounts of chlorite or epidote, Fe-carbonates, Fe-hydroxides, and Fe^{3+}, Type 1 are mapped in the Eocene–Oligocene rocks (lat 33°23′15.94″N., long 62°7′8.54″E.) in the southern part of the AOI. Although the area has no obvious heat source, the mineral assemblage suggests possible hydrothermal alteration.

Spatially coherent concentrations of hematite occur over a broad swath in the central portion of the AOI. The spatially consistent patterns occur in late Quaternary and Recent, Pliocene, Eocene–Oligocene, and Miocene age rocks. In some areas the hematitic minerals occur with Fe-hydroxides. Hematites along this trend are associated with above mentioned buddingtonite occurrence near lat 33°42′42.28″N., long 62°0′12.55″E. to lat 33°40′58.76″N., long 61°56′58.47″E.).

A ring of epidote appears in close proximity to the Oligocene intrusion near lat 33°47′2.0″N., long 62°0′55.74″E. in Berriasian-Valanginian age rocks and warrants additional study.

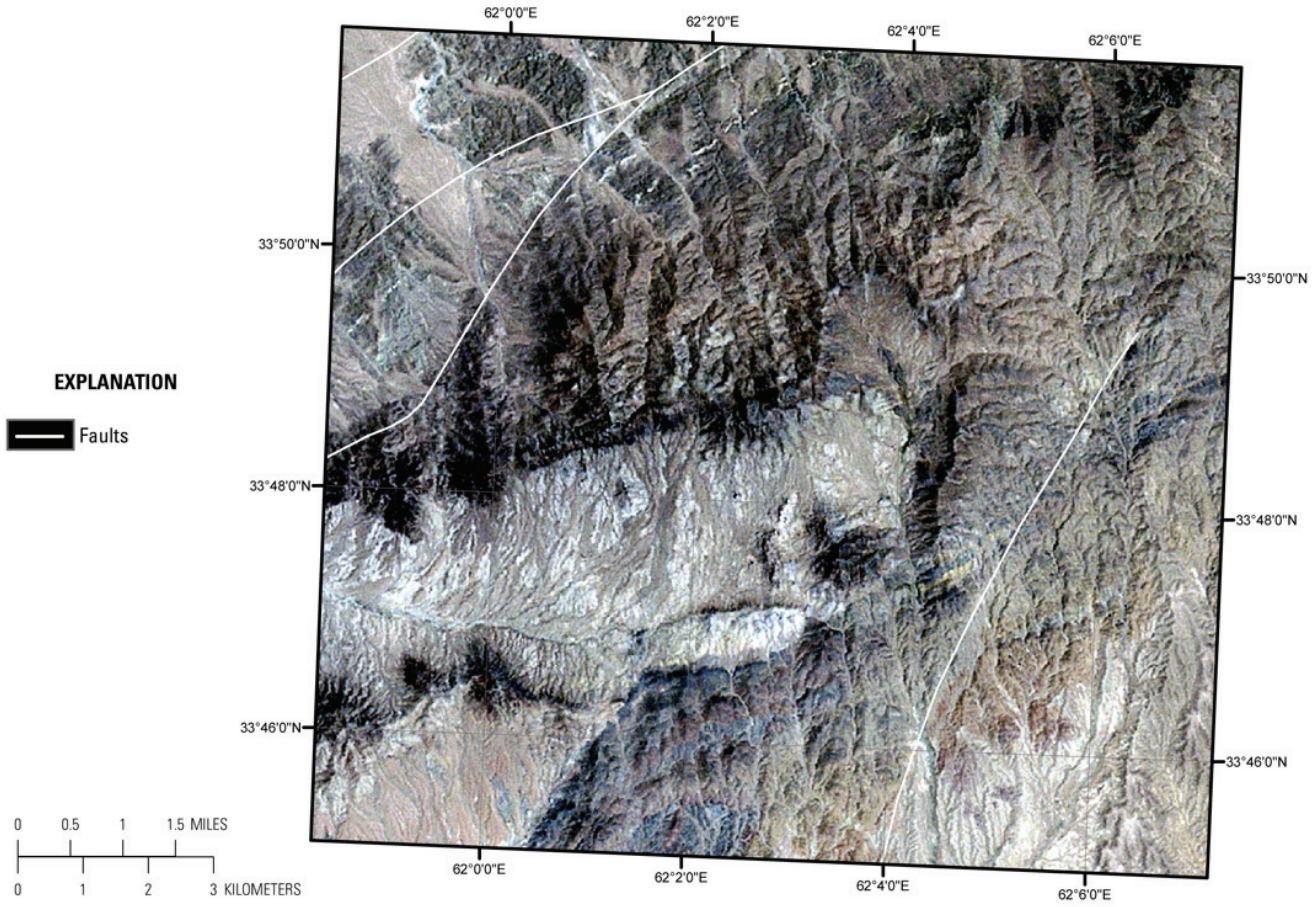

Figure 6B–27. Map showing Landsat Thematic Mapper data for the Dahana-Misgaran subarea (Davis, 2007).

6B.5.1 Shaida Subarea

Of the four previously identified areas of known mineralization (Shaida, Shaida I, Shaida II, and Shaida III), the Shaida II and Shaida III sites show the best correlation with the HyMap data. Shaida II and Shaida III are located in areas that show enrichment of chlorites or epidote (fig. 6B–20) and goethitic minerals (fig. 6B–21). All four recognized mineral prospects occur in areas where the HyMap data have detected Fe-hydroxides.

The HyMap data show spatially well-defined patterns of kaolinite and goethite-rich material along the northeast-trending fault trace originating near the Shaida volcanic massive sulfide (VMS) prospect. This spatially coherent group of kaolinitic and goethitic material occurs, along with illites and muscovite group minerals, in Late Jurassic–Early Cretaceous, Early Cretaceous, and Oligocene age rocks and should be a target for additional characterization as this mineral assemblage is commonly associated with epithermal processes (figs. 6B–20, 6B–21, and 6B–25).

Kaolinite, muscovite, goethite, and lesser amounts of Fe-hydroxide occur in spatially discrete groups along the contact zone between Eocene–Oligocene and Pliocene rocks east of the Eocene–Oligocene intrusions near lat 66°53′10.86″E., long 33°25′9.69″N. The mineral distribution pattern and proximity to the intrusive bodies make this a region of interest as mineralizing fluids may have been mobile along the geologic contacts.

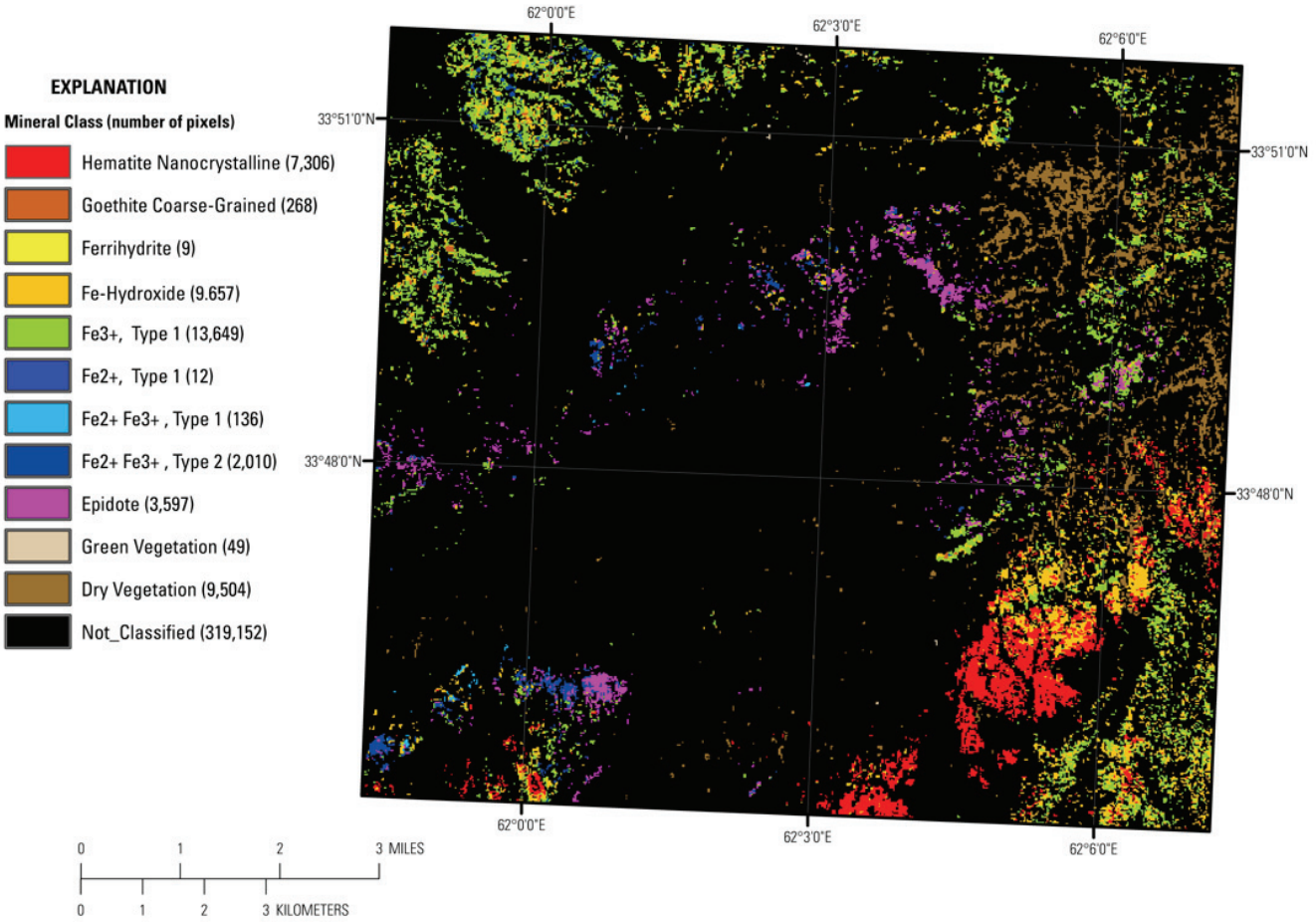

Figure 6B–28. Iron-bearing and other minerals detected in the HyMap data of the Dahana-Misgaran subarea.

Additional studies are needed to verify the presence and association of chlorite or epidote group, muscovites, illites (fig. 6B–20), and Fe^{2+} Fe^{3+}, Type 2 (fig. 6B–17), which occur together in the Late Jurassic–Early Cretaceous age rocks in the northwest part of the subarea near lat 61°48′27.96″E., long 33°55′38.76″N. to the northwest of the mapped Early Cretaceous and Oligocene age intrusions. On the basis of the HyMap and TM data, and considering that the currently mapped fault trace may in reality be shifted to the south, these spatially coherent groups of chlorite or epidote and Fe^{2+} Fe^{3+}, Type 2 minerals may occur adjacent to or near the actual fault trace.

Hematite and goethite pixels are also present in the north-central part of the subarea and may be associated with a misaligned northern fault trace. These spatially coherent mineral patterns are suggestive of limonitic alteration, which is known to be associated with tin mineralization (Peters and others, 2007).

A northeast-southwest trend (lat 33°42′42.28″N., long 62°0′12.55″E. to 33°40′58.76″N., 61°56′58.47”E.) of buddingtonite is present in the Eocene–Oligocene rocks in the western half of the AOI. The buddingtonite occurs intermixed with kaolinite, hematite, goethite, and Fe-hydroxides. This mineral assemblage is suggestive of advanced argillic alteration, and the area should be subjected to additional geochemical, geological, and geophysical evaluation.

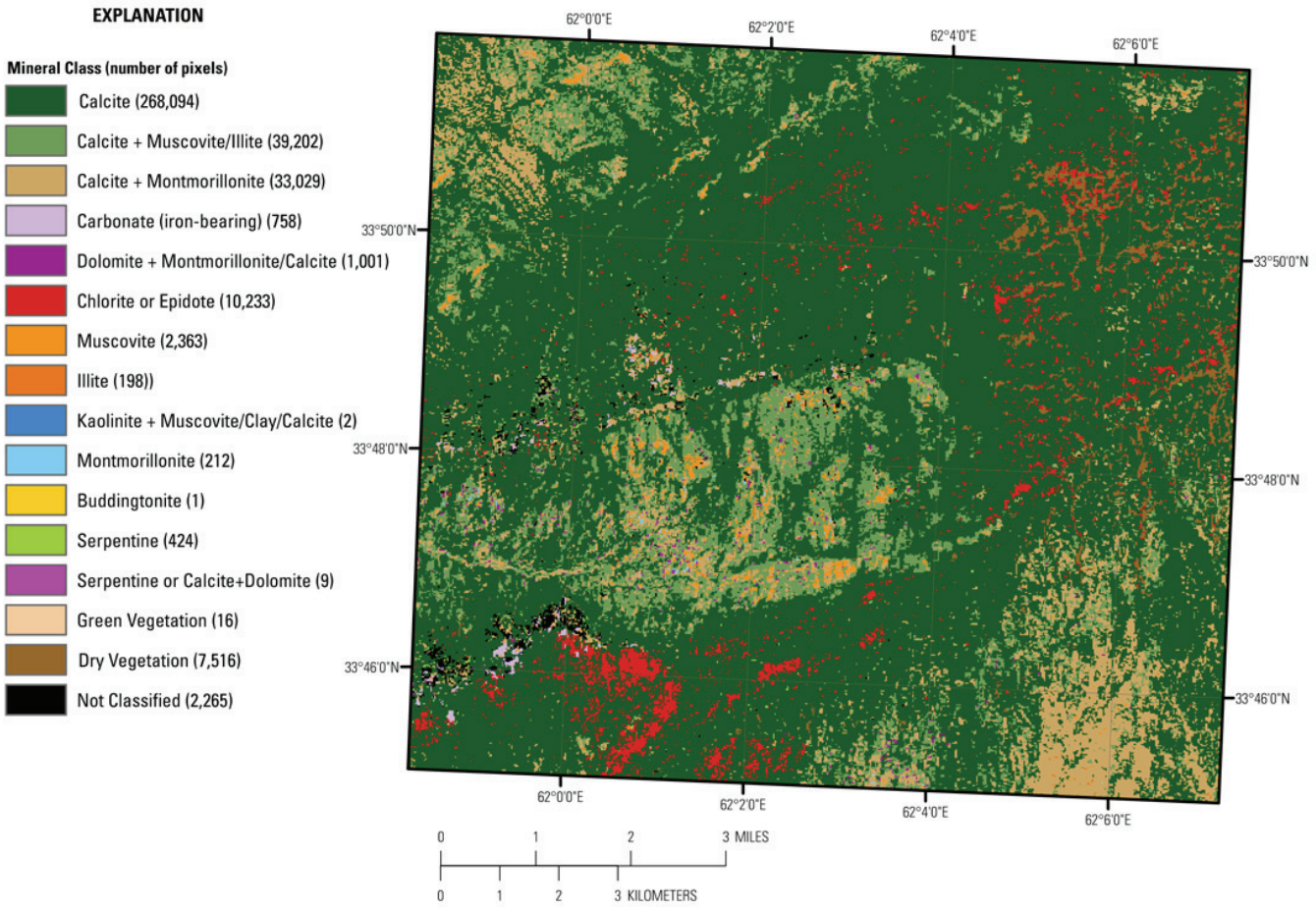

Figure 6B–29. Distribution of clays, carbonates, phyllosilicates, sulphates, and other alteration minerals for the Dahana-Misgaran subarea based on the HyMap data.

Abundant buddingtonite is associated with Fe-hydroxide, Fe^{3+}, Type 1, and lesser amounts of chlorite or epidote, Fe-carbonates, and hematite in the Eocene–Oligocene rocks (lat 33°23′15.94″N., long 62°7′8.54″E.) in the southern part of the AOI (figs. 6B–6 and 6B–7). The spatial extent of the buddingtonite pixels and the presence of other alteration minerals suggest potential epithermal mineralization (see King, Johnson, and others, 2011).

Hematitic minerals occur in large concentrations along a southwest to northeast trend in the center of the AOI primarily in Pliocene, Eocene–Oligocene, and Miocene age rocks. The hematitic minerals are commonly associated with Fe-hydroxides in the Pliocene age rocks. The widespread occurrence across various geologic units makes this an interesting target for further investigation.

6B.5.2 Dahana-Misgaran Subarea

The HyMap data suggest that the size of the mapped Oligocene intrusion in the Dahana-Misgaran subarea is larger than what has previously been mapped. Figures 6B–29 and 6B–33 best show the mineral distribution patterns that define a contact zone around what seems to be an intrusive body. In figure 6B–29, the margin of the intrusive body is distinguished by the Fe-bearing carbonates and carbonate mineral mixtures in primarily calcite host rocks. In figure 6B–33, the spatial distribution of epidote marks a margin of a seemingly single intrusive body. The underlying shaded relief and the TM map (fig. 6B–27) suggest either a single large intrusion or two separate intrusions; one that is oriented primarily east-west that is similar in shape to the currently mapped intrusion, and a smaller north-south body on the eastern edge of the presently mapped Oligocene intrusive unit. If two intrusive units are present, they are not necessarily the same geologic age.

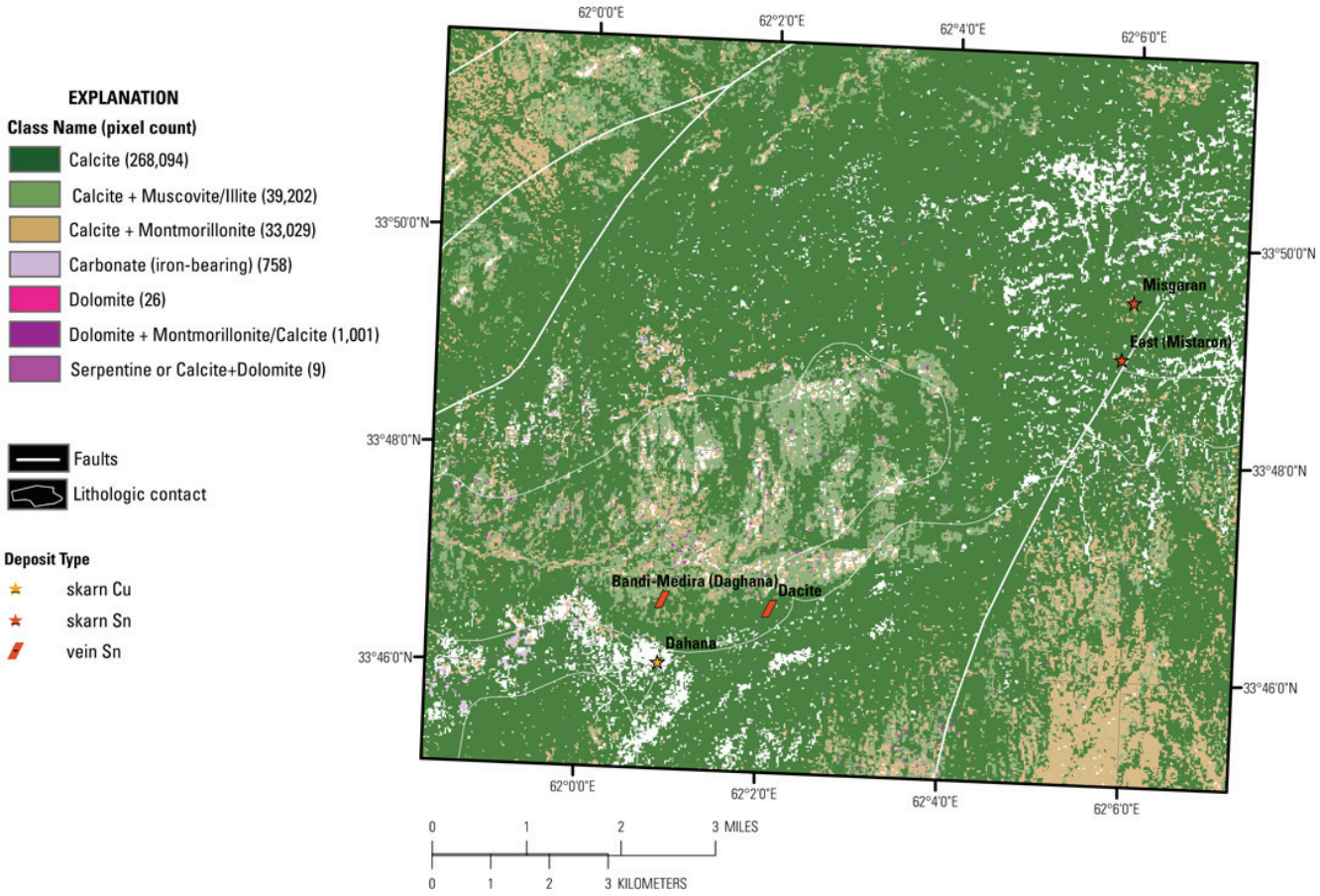

Figure 6B–30. Distribution of carbonate-bearing minerals in Dahana-Misgaran subarea detected in the HyMap data.

Iron-bearing carbonates are clustered north of the known mapped intrusion and have been tagged as an area that warrants additional geochemical and geophysical evaluation (King, Johnson, and others, 2011). Iron-bearing carbonates are also clustered in the Berriasian–Valanginian rocks west of the Dahana mineral occurrence and south of the mapped intrusive rocks (fig. 6B–34). Their presence combined with the Fe-hydroxides, chlorites or epidote, and epidote makes this an attractive area for supportive investigations.

Hematite and Fe-hydroxides in the Pliocene rocks (southeastern part of the subarea, south of the fault trace terminating near the East Mistaron site) correlate with reddish colored terrain in the Landsat TM image and warrant additional geochemical characterization.

Only the East Mistaron and Dahana prospects occur in areas with minerals detected and mapped by the HyMap data.

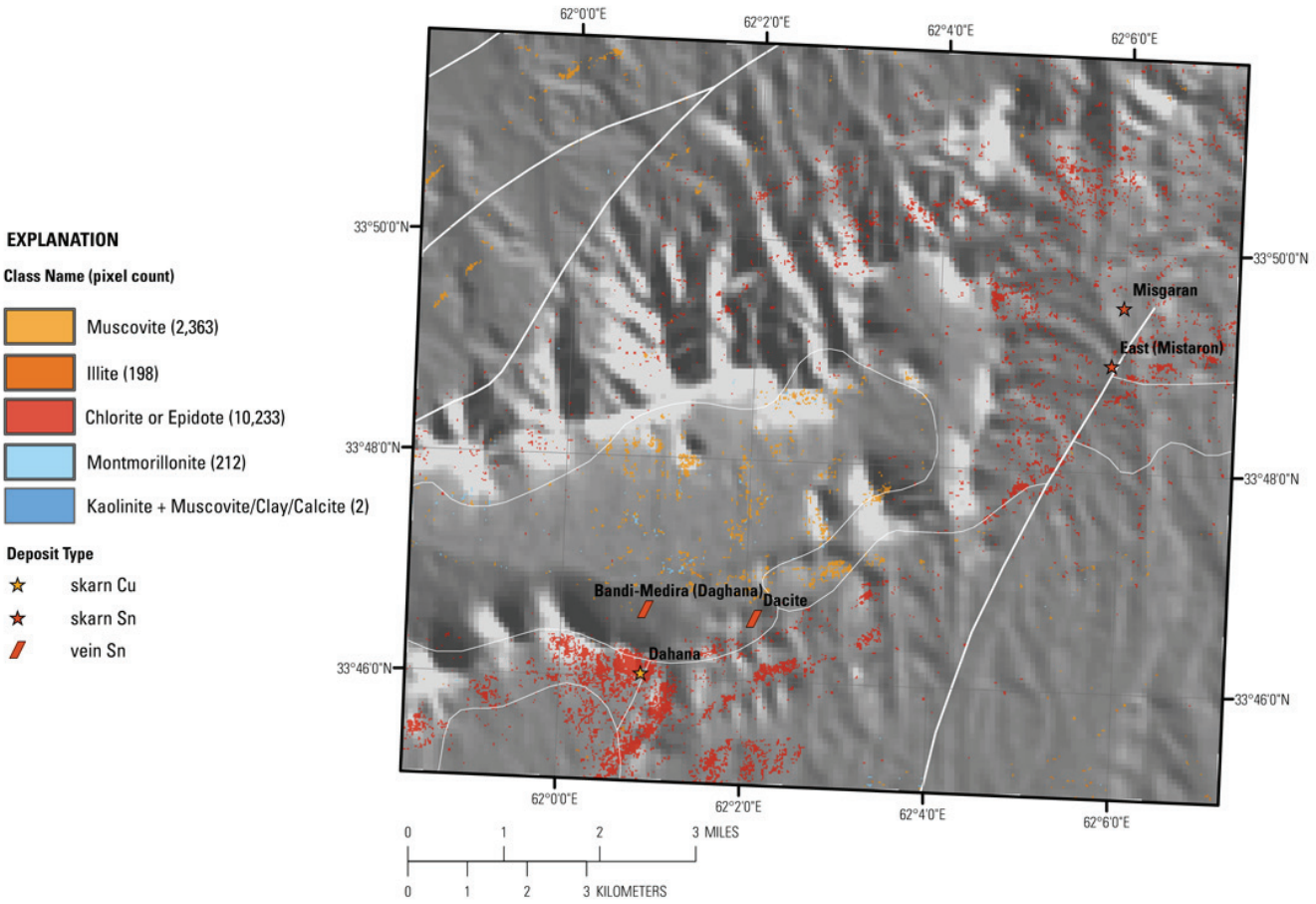

Figure 6B–31. Distribution of clays and micas in the Dahana-Misgaran subarea using the HyMap data.

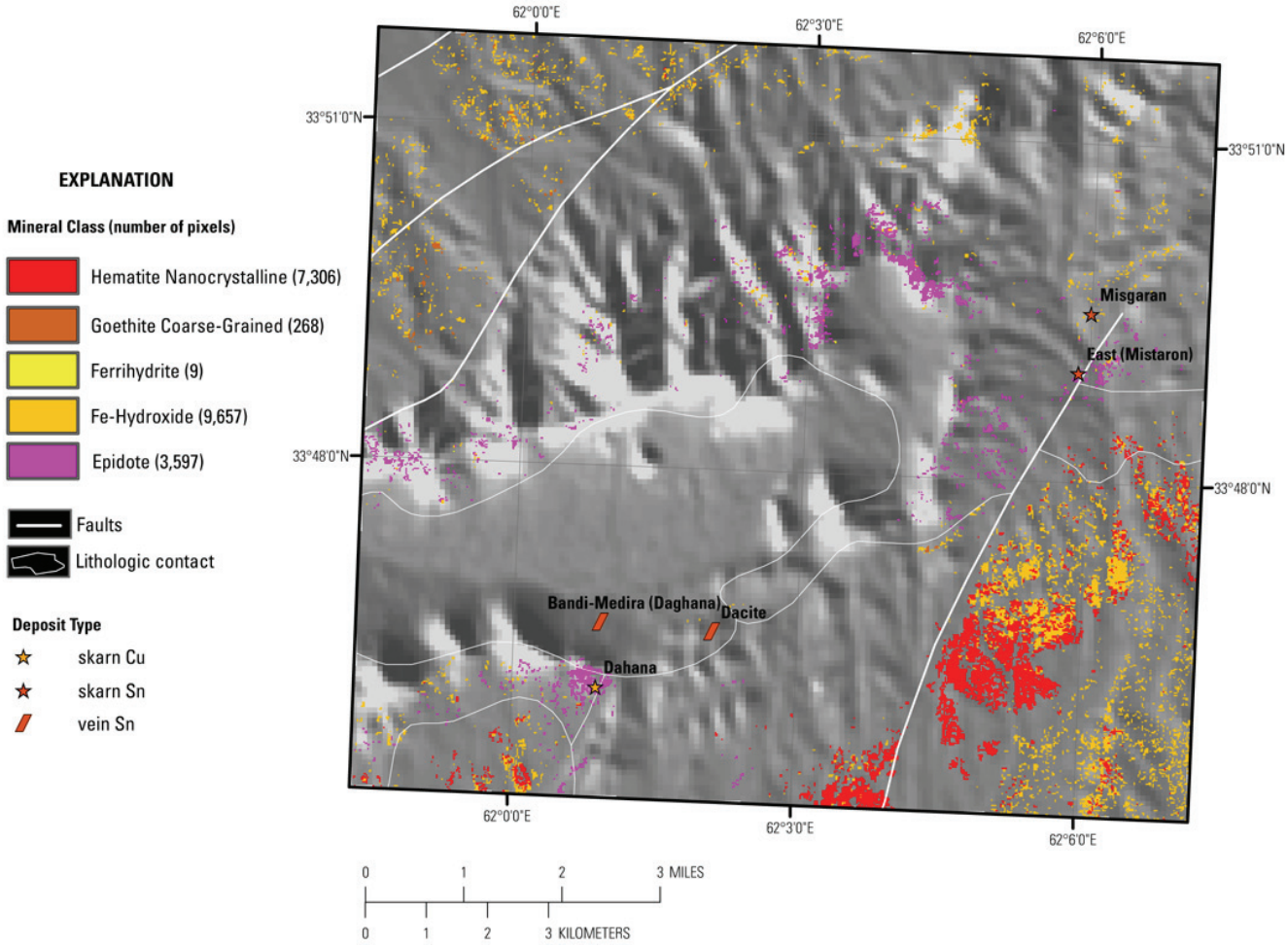

Figure 6B–32. Distribution of iron-hydroxides and iron-oxides for the Dahana-Misgaran subarea.

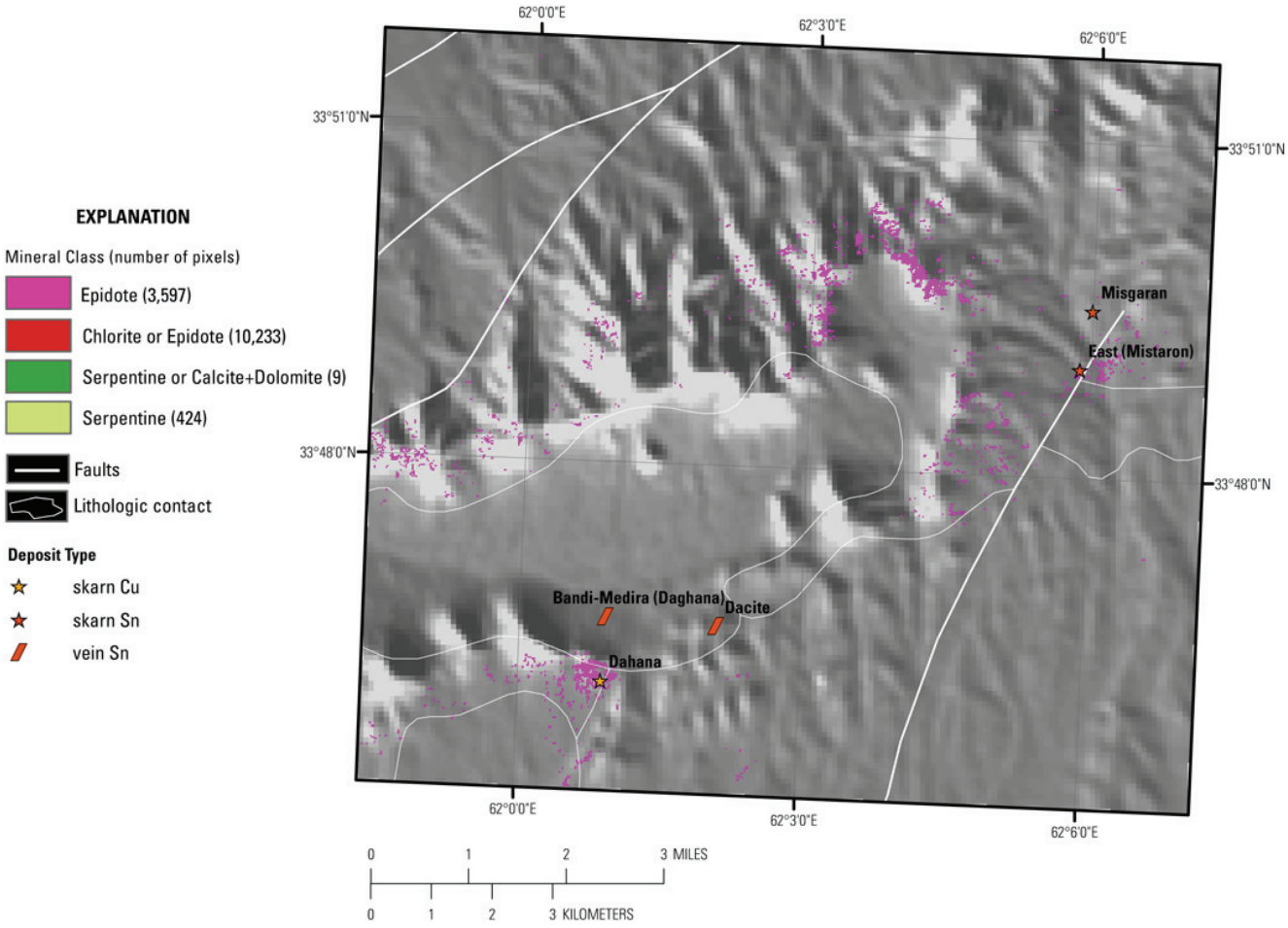

Figure 6B–33. Occurrence and distribution of common secondary minerals detected in the HyMap data for Dahana-Misgaran subarea.

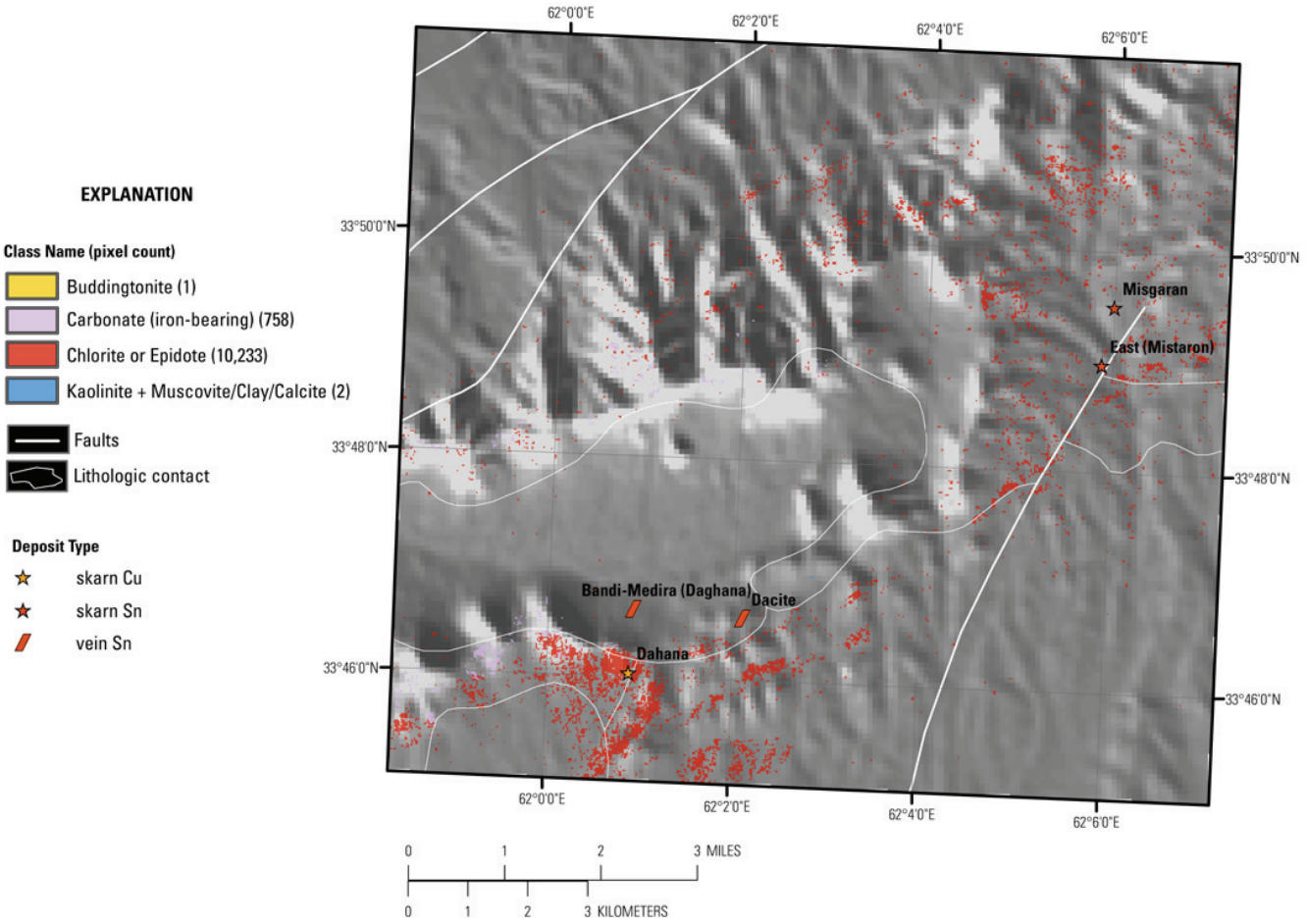

Figure 6B–34. Common alteration materials detected in the HyMap data are shown on this map for the Dahana-Misgaran subarea.

6B.6 References Cited

Abdullah, Sh., and Chmyriov, V.M., 1977, Geological map of Afghanistan: Kabul, Afghanistan, Ministry of Mining and Industry of the Democratic Republic of Afghanistan, scale 1:500,000.

Cocks, T., Jenssen, R., Stewart, A., Wilson, I., and Shields, T., 1998, The HyMap airborne hyperspectral sensor—The system, calibration and performance, *in* Schaepman, M., Schlapfer, D., and Itten, K.I., eds., Proceedings of the 1st EARSeL Workshop on Imaging Spectroscopy, 6–8 October 1998, Zurich: Paris, European Association of Remote Sensing Laboratories, p. 37–43.

Davis, P.A., 2007, Landsat ETM+ false-color image mosaics of Afghanistan: U.S. Geological Survey Open-File Report 2007–1029, 22 p. (Also available at *http://pubs.usgs.gov/of/2007/1029/*.)

Doebrich, J.L., and Wahl, R.R., comps., *with contributions by* Doebrich, J.L., Wahl, R.R., Ludington, S.D., Chirico, P.G., Wandrey, C.J., Bohannon, R.G., Orris, G.J., Bliss, J.D., and ____, 2006, Geologic and mineral resource map of Afghanistan: U.S. Geological Survey Open File Report 2006–1038, scale 1:850,000, available at *http://pubs.usgs.gov/of/2006/1038/*.

Dronov, V.I., Kalimulin, S.M., Sborshchikov, I.M., Svezhentsov, V.P., Chistyakov, A.N., Zelensky, E.D., and Cherepov, P.G., 1972, The geology and minerals of North Afghanistan (parts of map sheets 400-II and 500-I, the Kaysar-Hari Rod Interfluve area): [Afghanistan] Department of Geological and Mineral Survey, 44 p.

Hoefen, T.M., Kokaly, R.F., and King, T.V.V., 2010, Calibration of HyMap data covering the country of Afghanistan, *in* Proceedings of the 15th Australasian Remote Sensing and Photogrammetry Conference, Alice Springs, Australia, September 12–17, 2010, p. 409, available at *http://dl.dropbox.com/u/81114/15ARSPC-Proceedings.zip/*.

King, T.V.V., Kokaly, R.F., Hoefen, T.M., and Knepper, D.H., 2010, Resource mapping in Afghanistan using HyMap data, *in* Proceedings of the 15th Australasian Remote Sensing and Photogrammetry Conference, Alice Springs, Australia, September 12–17, 2010, p. 500, available at *http://dl.dropbox.com/u/81114/15ARSPC-Proceedings.zip/*.

King, T.V.V., Johnson, M.R., Hoefen, T.M., Kokaly, R.F., and Livo, K.E., 2011, Mapping potential mineral resource anomalies using HyMap data, *in* King, T.V.V., Johnson, M.R., Hubbard, B.E., and Drenth, B.J., eds, Identification of mineral resources in Afghanistan—Detecting and mapping resource anomalies in prioritized areas using geophysical and remote sensing (ASTER and HyMap) data in Afghanistan: U.S. Geological Survey Open-File Report 2011–1229, available at *http://pubs.usgs.gov/of/2011/1229/*.

King, T.V.V., Kokaly, R.F., Hoefen, T.M., Dudek, K. and Livo, K.E., 2011, Surface materials map of Afghanistan—Iron-bearing minerals and other materials: U.S. Geological Survey Scientific Investigations Map 3152–B.

Kokaly, Ray, 2011, PRISM—Processing routines in IDL for spectroscopic measurements: U.S. Geological Survey Open-File Report 2011–1155, available at *http://pubs.usgs.gov/of/2011/1155/*.

Kokaly, R.F., King, T.V.V., and Livo, K.E., 2008, Airborne hyperspectral survey of Afghanistan 2007—Flight line planning and HyMap data collection: U.S. Geological Survey Open-File Report 2008–1235, 14 p.

Kokaly, R.F., King, T.V.V., Hoefen, T.M., Dudek, K. and Livo, K.E., 2011, Surface materials map of Afghanistan—Carbonates, phyllosilicates, sulfates, altered minerals, and other materials: U.S. Geological Survey Scientific Investigations Map 3152–A.

Peters, S.G., Ludington, S.D., Orris, G.J., Sutphin, D.M., Bliss, J.D., and Rytuba, J.J., eds., and the U.S. Geological Survey-Afghanistan Ministry of Mines Joint Mineral Resource Assessment Team, 2007, Preliminary non-fuel mineral resource assessment of Afghanistan: U.S. Geological Survey Open-File Report 2007–1214, 810 p., 1 CD–ROM. (Also available at *http://pubs.usgs.gov/of/2007/1214/*.)